Electronic Supplementary Material (ESI) for Chemical Science.
This journal is © The Royal Society of Chemistry 2014

Effective Sensing of RDX via Instant and Selective Detection of Ketone Vapors

Zhichao Hu,[†] Kui Tan,[‡] William P. Lustig,[†] Hao Wang,[†] Yonggang Zhao,[†] Chong Zheng,[§] Debasis Banerjee,[†] Thomas J. Emge,[†] Yves J. Chabal,[‡] and Jing Li*,[†]

[†] Department of Chemistry and Chemical Biology, Rutgers University, 610 Taylor Rd., Piscataway, NJ 08854

[‡] Department of Material Science and Engineering, University of Texas-Dallas, Richardson, TX 75080

[§] Department of Chemistry and Biochemistry, Northern Illinois University, DeKalb, IL 60115

Supporting Information

Table of Contents

1. Synthesis

Synthesis of $Zn_2(ofdc)_2(bpy)\cdot 2.5DMF\cdot 1.25H_2O$ (LMOF-201): $Zn(NO_3)_2\cdot 6H_2O$ (0.0297 g, 0.1 mmol), 9-fluorenone-2,7-dicarboxylic acid (0.0268 g, 0.1 mmol) and 4,4'-bipyridine (0.0156 g, 0.1 mmol) were dissolved in 10 mL N,N'-dimethylformamide (DMF) in a 20 ml glass vial. The mixture was sonicated for 10 min under room temperature. The sealed glass vial was then placed in a 100 °C oven for 2 days. Transparent yellow crystals were collected using filtration, washed with DMF and diethyl ether, then dried in air (Yield: ~40% based on ofdc).

Synthesis of $Zn_2(hfdc)_2(bpy)\cdot xDMA$ (LMOF-202): $Zn(NO_3)_2\cdot 6H_2O$ (0.0297 g, 0.1 mmol), 9H-fluorene-2,7-dicarboxylic acid (0.0254 g, 0.1 mmol) and 4,4'-bipyridine (0.0156 g, 0.1 mmol) were dissolved in 10 mL N,N'-dimethylacetamide (DMA) in a 20 ml glass vial. The mixture was sonicated for 10 min under room temperature. The sealed glass vial was then placed in a 120 °C oven for 2 days. Transparent orange yellow crystals were collected using filtration, washed with DMF and dichloromethane, then dried in air (Yield: ~40% based on hfdc).

Synthesis of $Zn_2(oba)_2(bpy)\cdot DMA$[1] (LMOF-121): $Zn(NO_3)_2\cdot 6H_2O$ (0.1487 g, 0.5 mmol), 4,4'-oxybis(benzolate) (0.1291 g, 0.5 mmol) and 4,4'-bipyridine (0.0781 g, 0.5 mmol) were dissolved in 10 mL N,N'-dimethylacetamide (DMA) in a 20 ml glass vial. The mixture was sonicated for 10 min under room temperature. The sealed glass vial was then placed in a 120 °C oven for 2 days. Transparent light yellow crystals were collected using filtration, washed with DMF and then dried in air.

2. Power X-ray diffraction, Thermogravimetric, and Elemental Analysis

Power X-ray diffraction (PXRD) patterns were collected on both as-made and outgassed samples on a Rigaku Ultima-IV diffractometer. The patterns were collected between 3° and 50° of the 2θ at a scan speed of 3 deg/min.

Thermogravimetric (TG) analysis was carried out on a TA Q5000 thermogravimetric analyzer. The compounds were activated by heating at elevated temperature (120 °C for LMOF-201 and -202; 150 °C for LMOF-121) under nitrogen flow (20 mL/min) until a constant weight loss.

Elemental analysis (EA) on fresh LMOF-201 and -202 samples were performed at the Robertson Microlit Laboratories in Ledgewood, New Jersey. The mass fractions (%) for C, H, and N are 53.32, 4.80, and 7.46 respectively, which account for 4 DMF and 3 water

molecules per unit cell (theoretically C% = 53.57, H% = 4.67, and N% = 7.21). For LMOF-202, the mass fractions (%) for C, H, and N are 56.37, 5.35, and 7.35 respectively, which account for 4 DMA and 3 water molecules per unit cell (theoretically C% = 56.34, H% = 5.57, and N% = 7.04).

The TG profile of LMOF-201 (Figure S3) shows a 28.3% weight loss at ~200 °C, which matches with the calculated 29.8% weight loss (using solvent amount indicated by EA). The TG profile of LMOF-202 (Figure S4) shows a 32.8% weight loss near 200 °C, which also matches with the calculated 33.7% weight loss (using solvent amount indicated by EA). The TG profiles of activated samples LMOF-201' and -202' both show flat regions before the structures collapse, indicating the complete removal of guest solvent molecules. The discrepancy between the solvent amount calculated from EA and single crystal data (section **3**) may due to that (i) solvents partially evaporate while in line for single crystal analysis or (ii) solvents are highly disordered and an accurate modeling of all solvent molecules may not be possible.

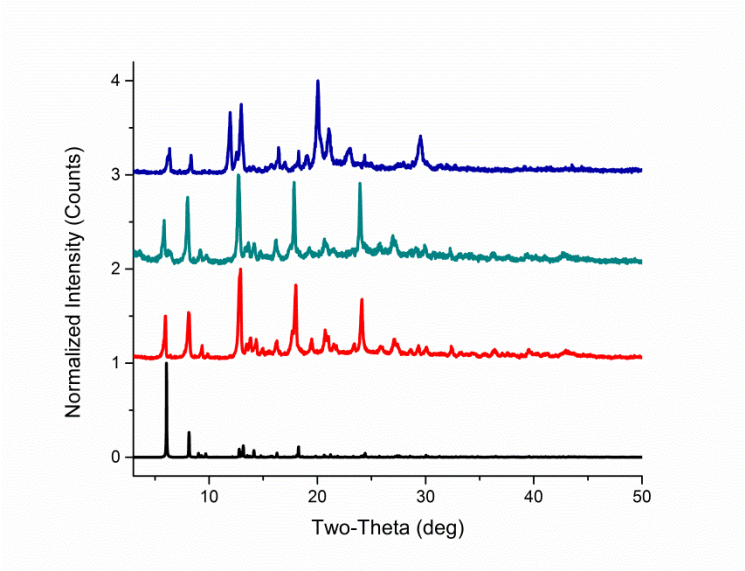

Figure S1. PXRD patterns of outgassed sample LMOF-201' (blue), diethyl ether washed sample (cyan), and as-made sample LMOF-201 (red) compared with the simulated pattern from the single crystal data (black).

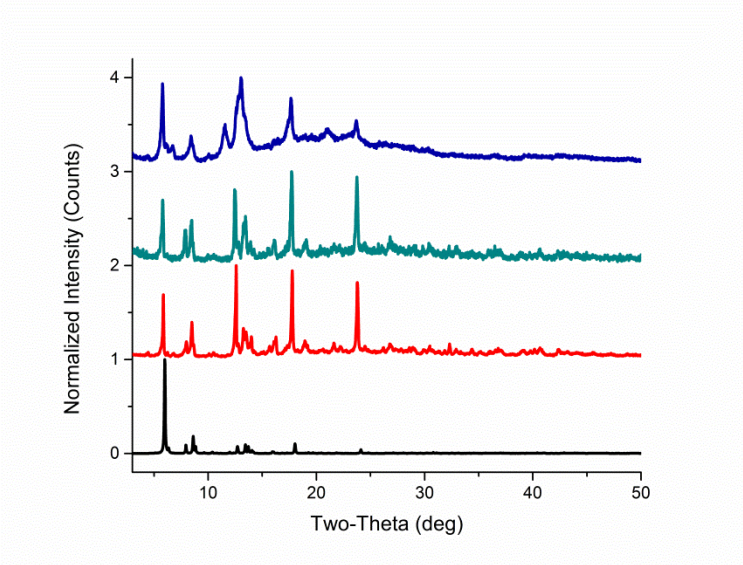

Figure S2. PXRD patterns of outgassed sample LMOF-202' (blue), dichloromethane washed sample (cyan), and as-made sample LMOF-202 (red) compared with the simulated pattern from the single crystal data (black).

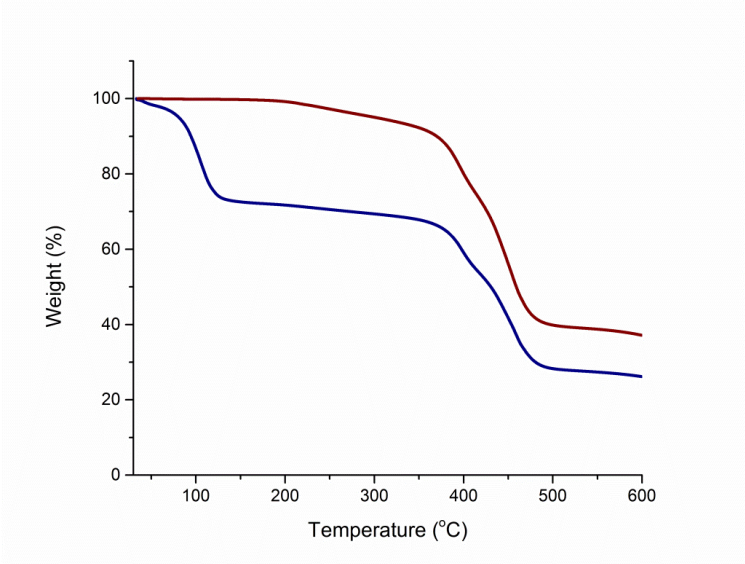

Figure S3. Thermogravimetric profile of LMOF-201 (blue) and LMOF-201' (burgundy) under nitrogen flow.

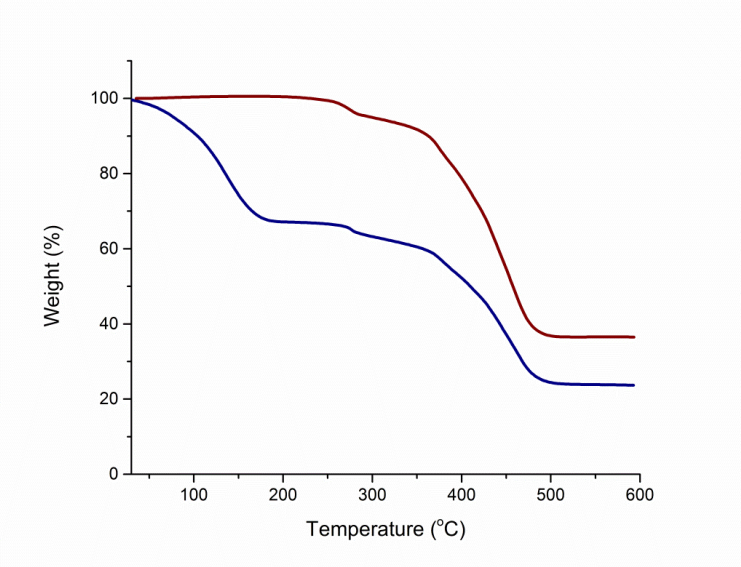

Figure S4. Thermogravimetric profile of LMOF-202 (blue) and LMOF-202' (burgundy) under nitrogen flow.

3. Single Crystal X-ray Diffraction Analysis

Single crystal X-ray diffraction data analysis of LMOF-201 and -202 were performed on a Bruker APEX-II CCD system with monochromized Mo Kα radiation (λ = 0.71073 Å). Crystal structures were solved by the SHELX97[2] program with the final full-matrix least-square refinement on F^2. Summaries of single crystal data are listed in Tables S1 to S4. Data for LMOF-202 were collected at two temperatures. However, the guest solvent molecules are still highly disordered at 100 K.

Table S1. Single crystal data for LMOF-201.

Compound	$[Zn_2(ofdc)_2(bpy)]\cdot 2.5DMF\cdot 1.25H_2O$ (LMOF-201)
Formula	$C_{47.5}H_{40}N_{4.5}O_{13.75}Zn_2$
M	1024.58
Crystal system	Monoclinic
Space group	P2(1)/c
a/Å	13.8166(7)
b/Å	21.7847(12)
c/Å	20.1414(11)

α/o	90.00
β/o	103.312(1)
γ/o	90.00
V, Å^3	5899.5(5)
Z	4
Temperature (K)	100(2)
λ (Mo Kα) Å	0.71073
D, g/cm^3	1.154
Reflections collected	59805
R1[a] [I > 2σ(*I*)]	0.0822
wR2[b] [I > 2σ(*I*)]	0.2006
Goodness-of-fit	1.017
CCDC number	979464

[a] $R1 = \sum |F_o - F_c| / \sum |F_o|$
[b] $wR2 = \sum[w(F_o^2 - F_c^2)^2] / w(F_o^2)^2]^{1/2}$

Table S2. Single crystal data for LMOF-202 at 295 K.

Compound	$[Zn_2(hfdc)_2(bpy)]\cdot x$DMA (LMOF-202)
Formula	$C_{40}H_{24}N_2O_8Zn_2$
M	791.39
Crystal system	Monoclinic
Space group	C 2/c
a/Å	33.559(7)
b/Å	22.171(4)
c/Å	19.706(4)
α/o	90.00
β/o	124.022(3)
γ/o	90.00
V, Å^3	12152(4)

Z	8
Temperature (K)	295(2)
λ (Mo Kα) Å	0.71073
D, g/cm^3	0.865
Reflections collected	47666
R1[a] [I > 2σ(*I*)]	0.0693
wR2[b] [I > 2σ(*I*)]	0.2322
Goodness-of-fit	1.048
CCDC number	979465

[a] $R1 = \sum |F_o - F_c| / \sum |F_o|$

[b] $wR2 = \sum[w(F_o^2 - F_c^2)^2] / w(F_o^2)^2]^{1/2}$

Table S3. Single crystal data for LMOF-202 at 295 K based on the PLATON/SQUEEZE model.[3]

Compound	$[Zn_2(hfdc)_2(bpy)]\cdot x$DMA (LMOF-202)
Formula	$C_{40}H_{24}N_2O_8Zn_2$
M	791.39
Crystal system	Monoclinic
Space group	C 2/c
a/Å	33.559(7)
b/Å	22.171(4)
c/Å	19.706(4)
α/o	90.00
β/o	124.022(3)
γ/o	90.00
V, Å^3	12152(4)
Z	8
Temperature (K)	295(2)
λ (Mo Kα) Å	0.71073
D, g/cm^3	0.865
Reflections collected	50481
R1[a] [I > 2σ(*I*)]	0.0436
wR2[b] [I > 2σ(*I*)]	0.1239
Goodness-of-fit	1.002
CCDC number	979466

[a] $R1 = \sum |F_o - F_c| / \sum |F_o|$

[b] $wR2 = \sum[w(F_o^2 - F_c^2)^2] / w(F_o^2)^2]^{1/2}$

Table S4. Single crystal data for LMOF-202 at 100 K.

Compound	$[Zn_2(hfdc)_2(bpy)]\cdot x$DMA (LMOF-202)
Formula	$C_{40}H_{21.61}N_2O_9Zn_2$
M	804.98
Crystal system	Monoclinic
Space group	C 2/c
a/Å	32.902(3)
b/Å	23.2587(18)
c/Å	18.5665(14)
α/o	90.00
β/o	122.0580(10)
γ/o	90.00
V, Å^3	12041.5(16)
Z	8
Temperature (K)	100(2)
λ (Mo Kα) Å	0.71073
D, g/cm^3	0.888
Reflections collected	46790
R1[a] [I > 2σ(*I*)]	0.0970
wR2[b] [I > 2σ(*I*)]	0.3194
Goodness-of-fit	1.047
CCDC number	979467

[a] $R1 = \sum |F_o - F_c| / \sum |F_o|$
[b] $wR2 = \sum[w(F_o^2 - F_c^2)^2] / w(F_o^2)^2]^{1/2}$

4. Gas Sorption and Pore Characterization

All gas sorption measurements were carried out on a volumetric gas sorption analyzer (Autosorb-1 MP, Quantachrome Instruments). Cryogenic temperature (77 K) was achieved by using liquid nitrogen as coolant. Ultra high purity N_2 (99.999%) was used in the sorption experiments. The N_2 sorption isotherms were collected in a relative pressure range from 10^{-6} to 1 at 77 K. Before each gas sorption measurement, around 100 mg as synthesized sample was activated at 393 K overnight under dynamic vacuum. Outgassed samples were used for gas sorption measurements and the weight of each sample was recorded before and after outgassing to confirm the removal of guest molecules. Pore properties (e.g. surface area and pore volume) were analyzed using Autosorb v1.50 software. The theoretical surface area is 745.0 m^2/g for LMOF-201, and 1664.5 m^2/g for LMOF-202 (calculated by Cerius2), which indicates LMOF-202 is intrinsically more porous than LMOF-201. The experimental results are listed in Table S5. The deviation between theoretical and experimental results is due to the structure change in activated samples.

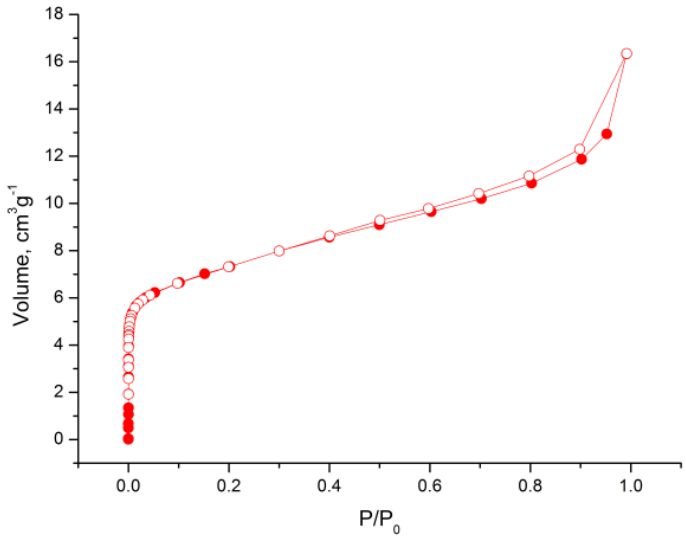

Figure S5. Nitrogen absorption (filled circle) and desorption (empty circle) of LMOF-201' at 77 K.

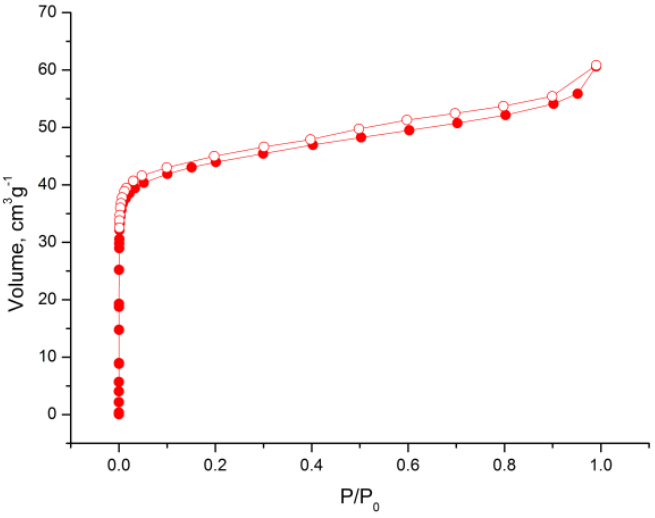

Figure S6. Nitrogen absorption (filled circle) and desorption (empty circle) of LMOF-202' at 77 K.

Table S5. Summary of pore properties of LMOF-201 and -202.

Compounds	BET surface area (m^2/g)	Pore Volume (cm^3/g)
$Zn_2(ofdc)_{2(}bpy)$	24.2	0.0251
$Zn_2(hfdc)_2(bpy)$	136	0.0932

Acetone adsorption measurements

Adsorption measurements were carried out using a modified Q-50 thermogravimetric analyzer (TA Instrument, Delaware). Nitrogen (Ultra High Pure, 99.999%) was used as carrier gas. The samples were activated at 120 and 150 °C for 5 hours for $Zn_2(hfdc)_2(bpy)$ and $Zn_2(oba)_2(bpy)$, respectively, in dry nitrogen prior to the adsorption experiments.

Isosteric heat of adsorption (Qst)

Acetone adsorption isotherms in three different temperatures (80, 90, and 100 °C) were used to calculate the Qst. The isotherms were fitted with Virial equation below:

$$\ln(p) = \ln(v) + (1/T)\sum_{i=0}^{m} a_i v^i + \sum_{j=0}^{n} b_j v^j$$

where *v*, *p*, and *T* are amount adsorbed, pressure, and temperature, respectively. The resultant a_i was used to calculate the Qst with the following equation:

$$Q_{st} = -R\sum_{i=0}^{m} a_i v^i$$

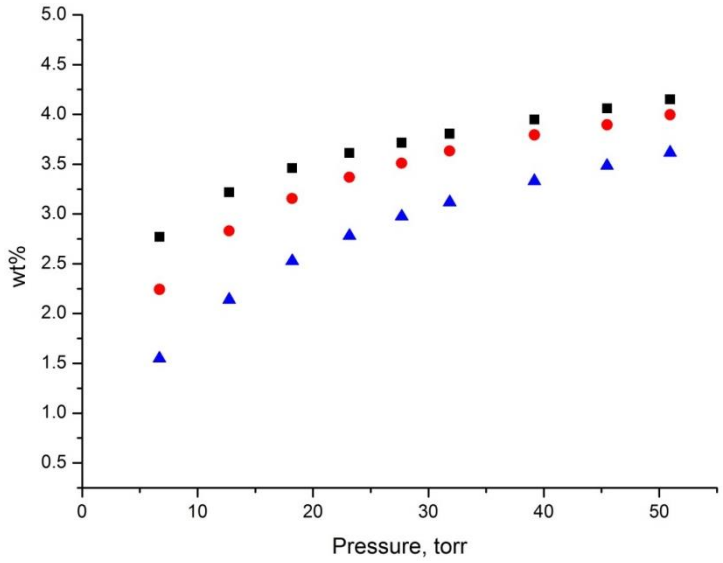

Figure S7. Acetone adsorption in LMOF-121 (Black: 80 °C, Red: 90 °C, and Blue: 100 °C).

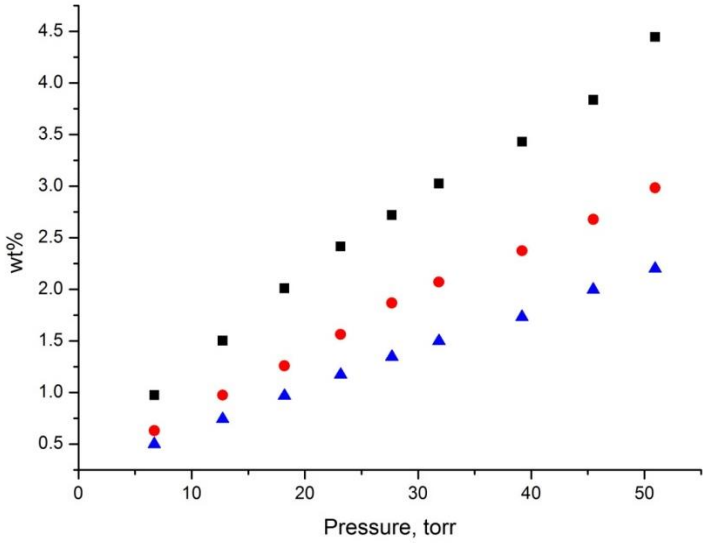

Figure S8. Acetone adsorption in LMOF-202 (Black: 80 °C, Red: 90 °C, Blue: 100 °C).

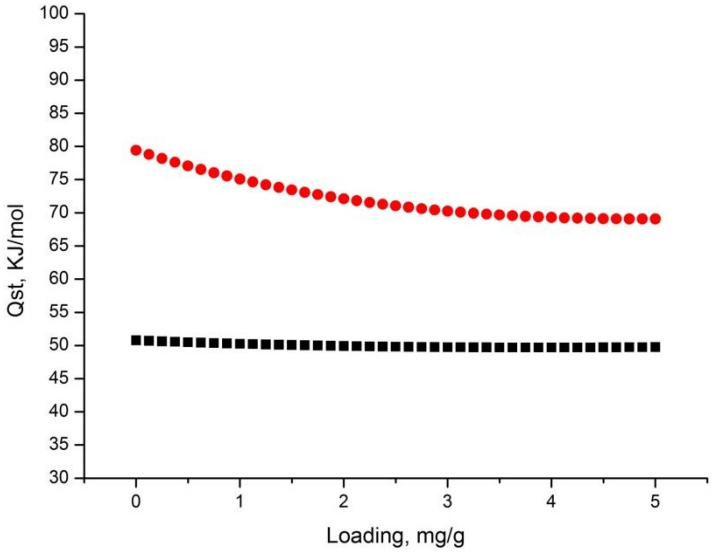

Figure S9. Heat of adsorption of acetone in LMOF-121 (red) and LMOF-202 (black).

5. Optical Absorption and Fluorescence Spectroscopy

The optical absorption spectra of solid samples were collected on a Shimadzu UV-3600 spectrophotometer at room temperature. The baseline was taken on a $BaSO_4$ standard. The diffuse reflectance was converted to Kubelka-Munk Function and the wavelength to eV.

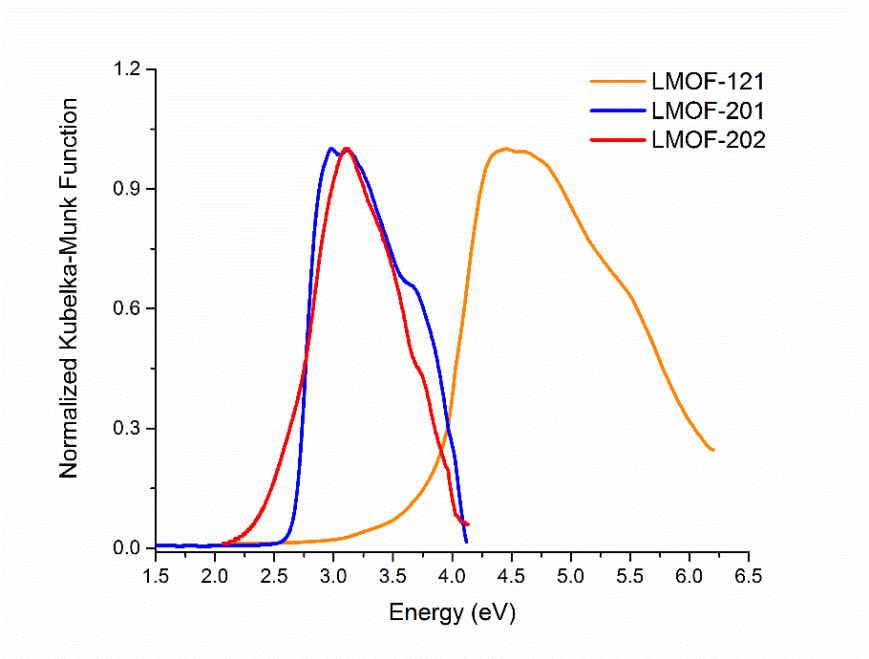

Figure S10. Optical adsorption spectra of solid samples of LMOF-121, LMOF-201, and LMOF-202.

The photoluminescence (PL) study was carried out on a Varian Cary Eclipse spectrophotometer at room temperature. Solid sample was ground into fine power and a layer of approximately 0.4 mg of the power was deposited on a glass slide (~1 cm × 5 cm). The sample slide was then exposed to the vapor of analyte in a closed jar. Fluorescence spectra were recorded before and after the exposure to vapors of different analytes for a selected time period at room temperature.

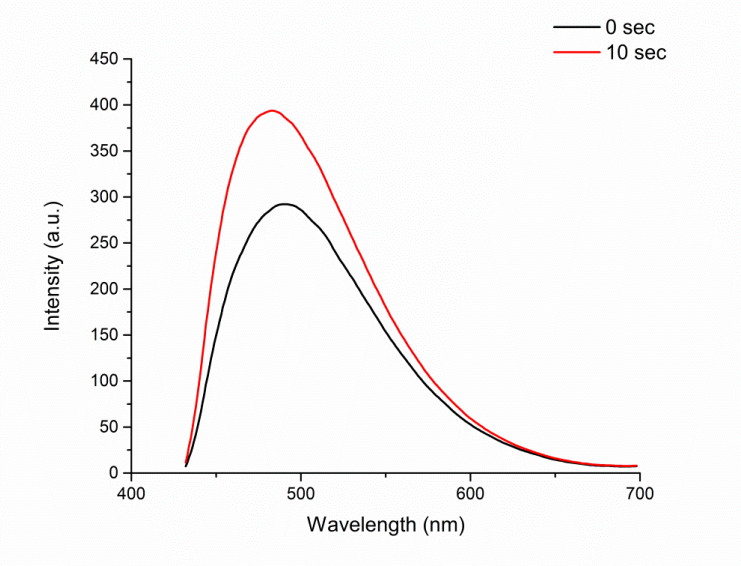

(a)

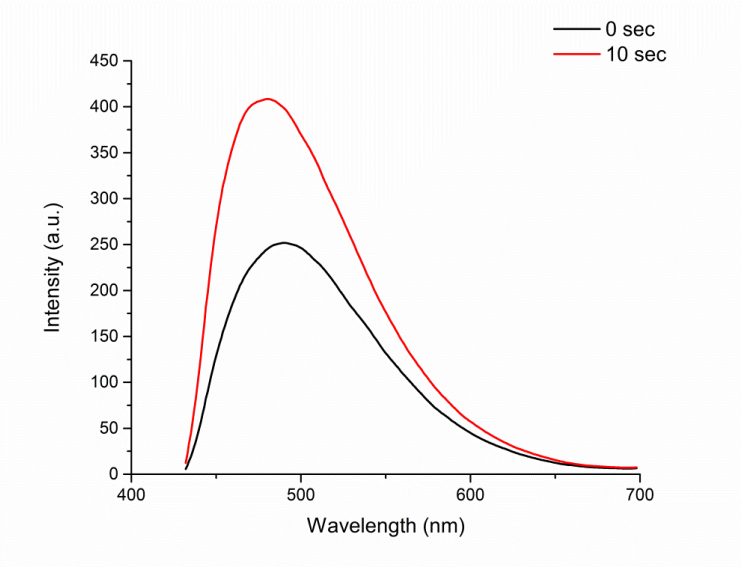
0 sec
10 sec
Intensity (a.u.)
Wavelength (nm)
0
50
100
150
200
250
300
350
400
450
400
500
600
700

(b)

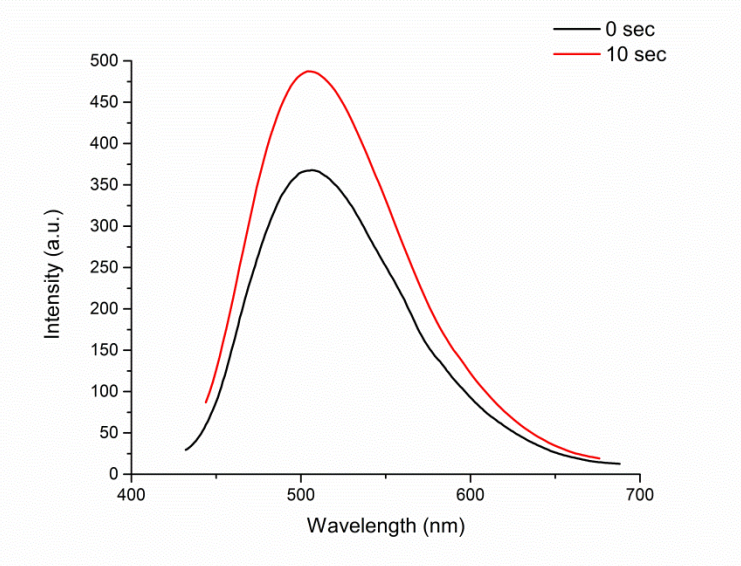
0 sec
10 sec
Intensity (a.u.)
Wavelength (nm)
0
50
100
150
200
250
300
350
400
450
500
400
500
600
700

(c)

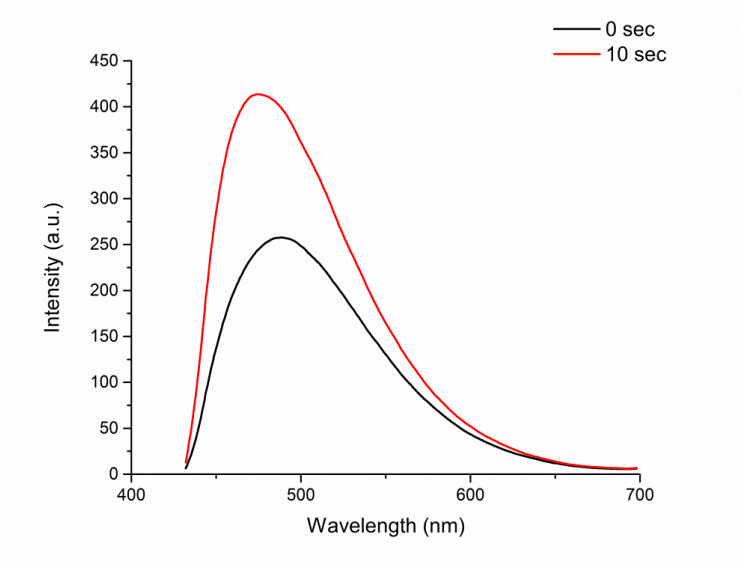
0 sec
10 sec
Intensity (a.u.)
Wavelength (nm)
0
50
100
150
200
250
300
350
400
450
400
500
600
700

(d)

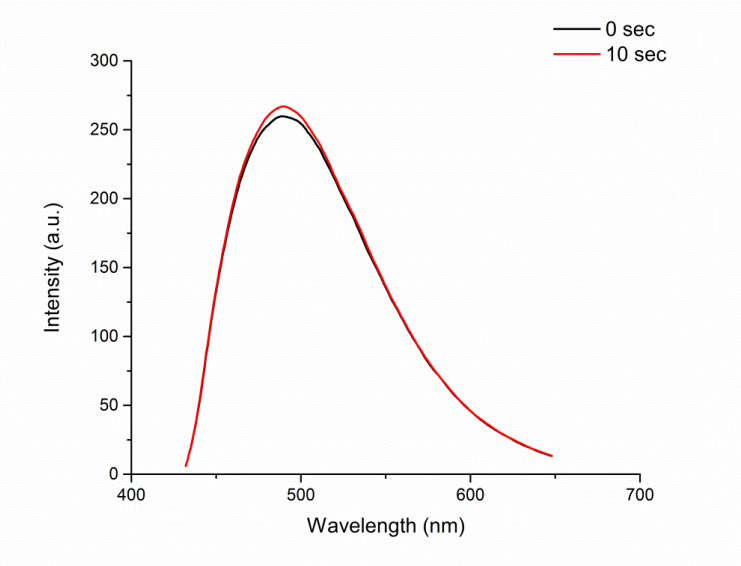
0 sec
10 sec
Intensity (a.u.)
Wavelength (nm)
0
50
100
150
200
250
300
400
500
600
700

(e)

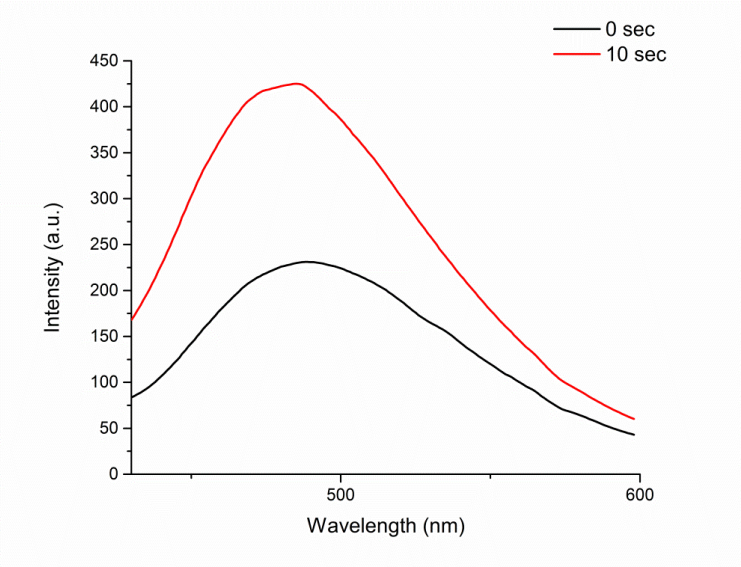
0 sec
10 sec
Intensity (a.u.)
Wavelength (nm)
0
50
100
150
200
250
300
350
400
450
500
600

(f)

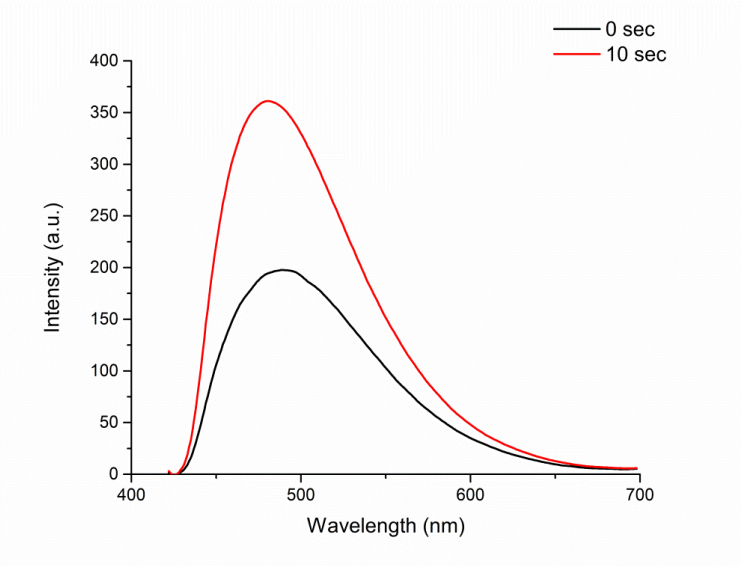
0 sec
10 sec
Intensity (a.u.)
Wavelength (nm)
0
50
100
150
200
250
300
350
400
400
500
600
700

(g)

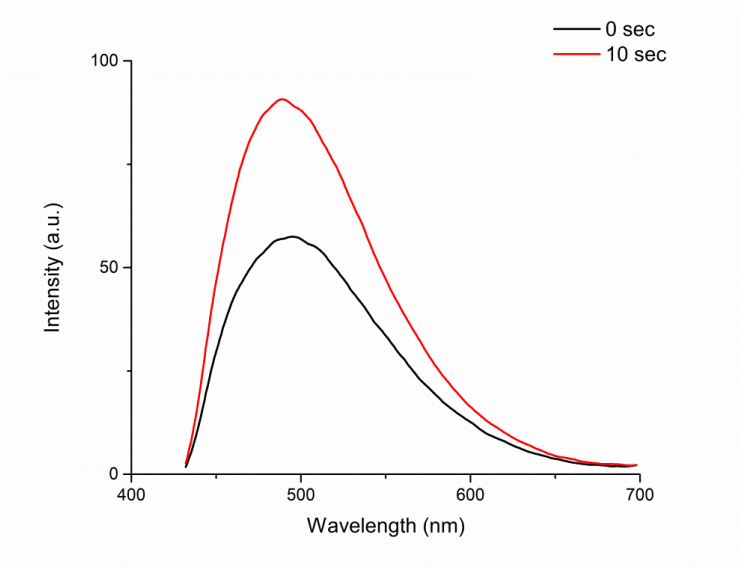

(h)

Figure S11. PL emission spectra of LMOF-202' (black) and the same sample after 10 s exposure to analytes (red) at room temperature: (a) 3-pentanone, (b) 2-octanone, (c) butanone, (d) 2,4-dimethyl-3-pentanone, (e)acetone, (f) cycloheptanone, (g) cyclopentanone, (h) cyclohexanone.

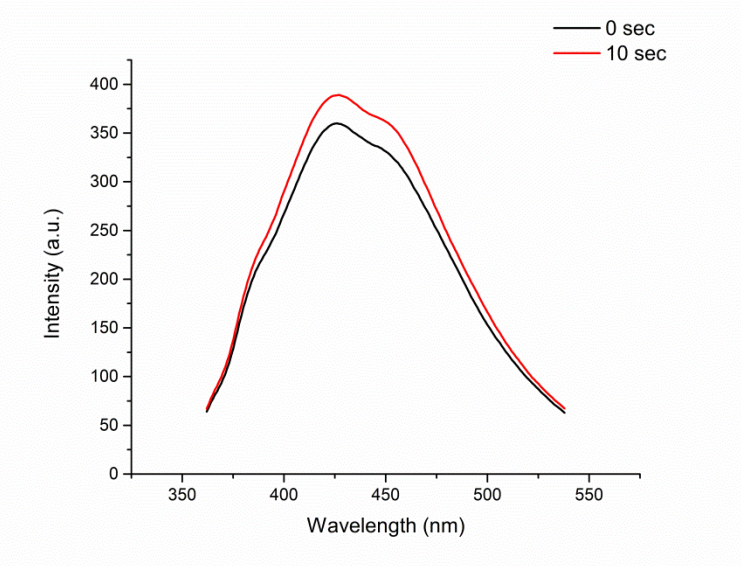

(a)

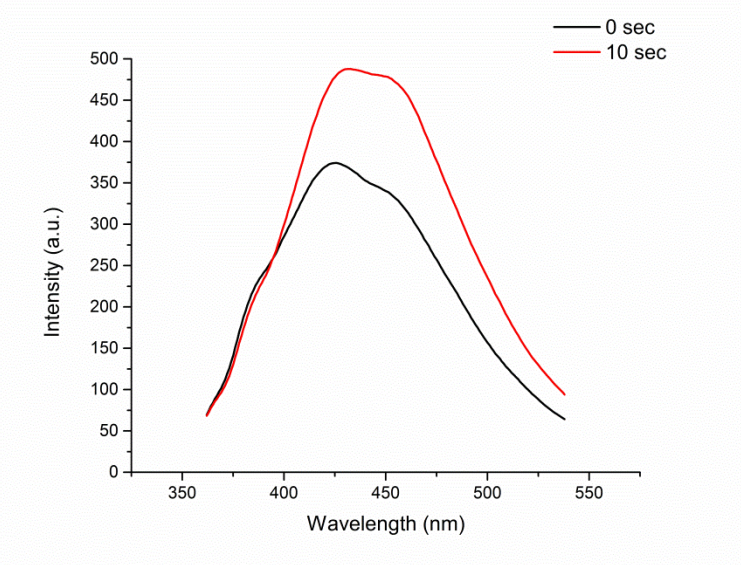
0 sec
10 sec
Intensity (a.u.)
Wavelength (nm)
0
50
100
150
200
250
300
350
400
450
500
350
400
450
500
550

(b)

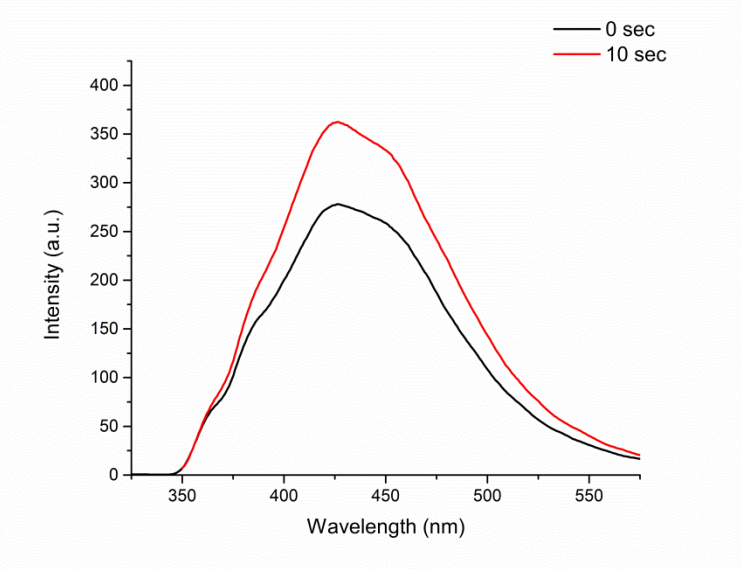
0 sec
10 sec
Intensity (a.u.)
Wavelength (nm)
0
50
100
150
200
250
300
350
400
350
400
450
500
550

(c)

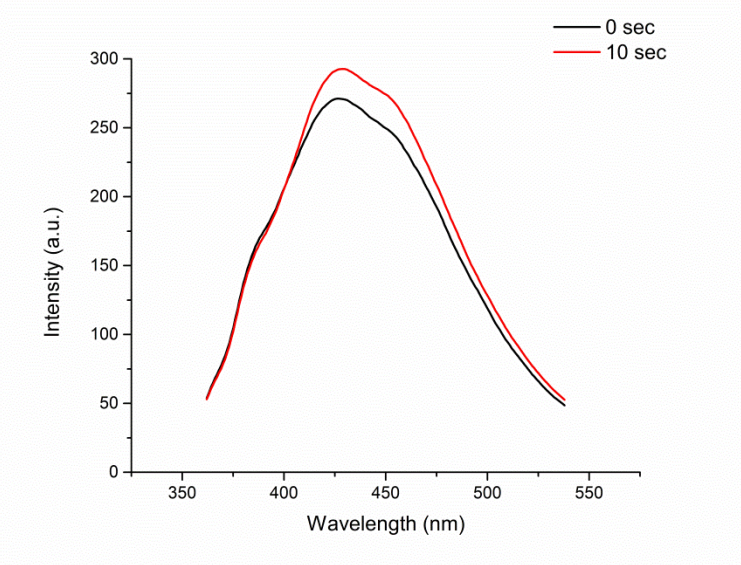
0 sec
10 sec
Intensity (a.u.)
Wavelength (nm)
0
50
100
150
200
250
300
350
400
450
500
550

(d)

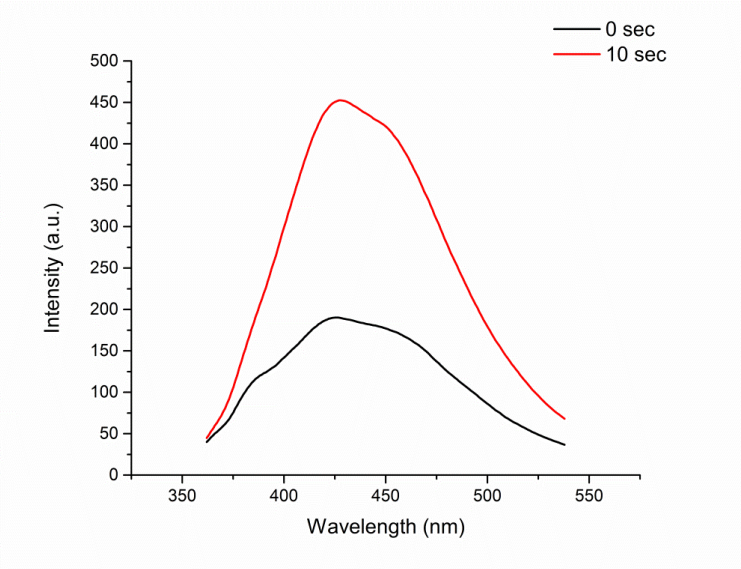
0 sec
10 sec
Intensity (a.u.)
Wavelength (nm)
0
50
100
150
200
250
300
350
400
450
500
550

(e)

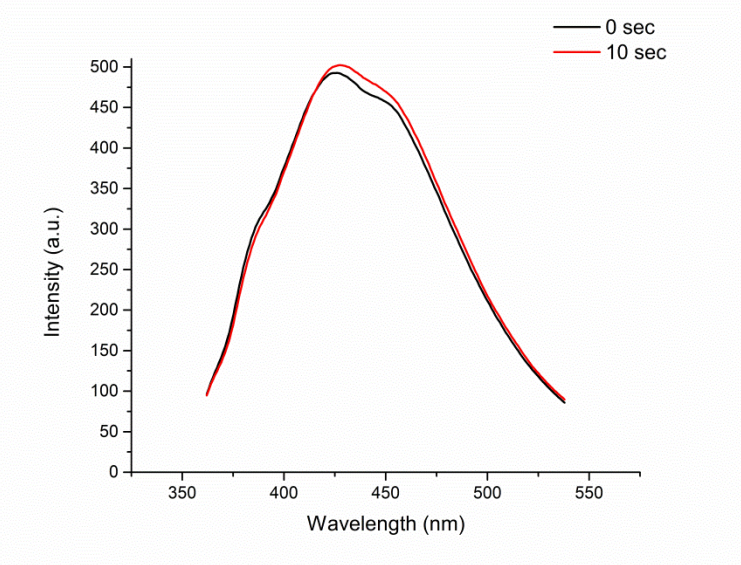
0 sec
10 sec
Intensity (a.u.)
Wavelength (nm)
0
50
100
150
200
250
300
350
400
450
500
350
400
450
500
550

(f)

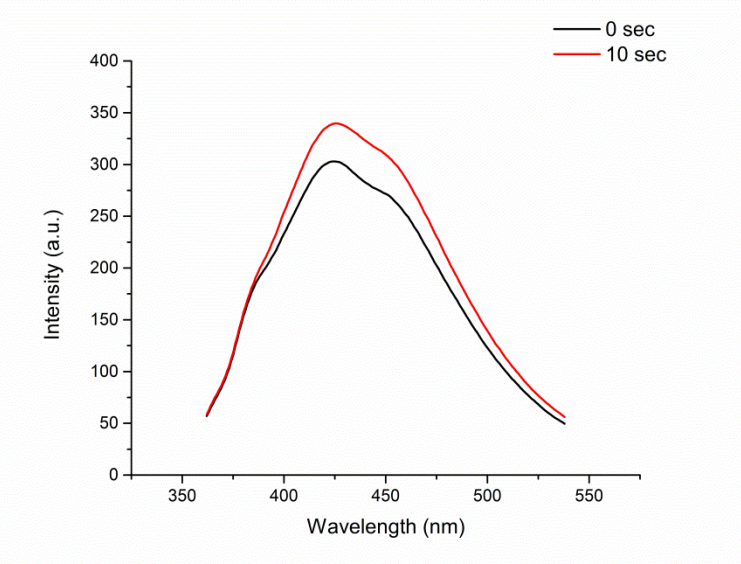
0 sec
10 sec
Intensity (a.u.)
Wavelength (nm)
0
50
100
150
200
250
300
350
400
350
400
450
500
550

(g)

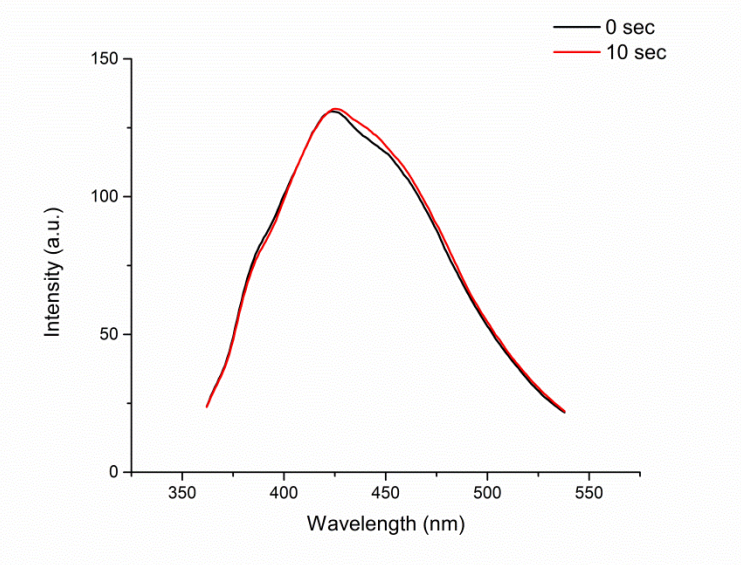

(h)

Figure S12. PL emission spectra of LMOF-121' (black) and the same sample after 10 s exposure to analytes (red) at room temperature: (a) 3-pentanone, (b) 2-octanone, (c) butanone, (d) 2,4-dimethyl-3-pentanone, (e)acetone, (f) cycloheptanone, (g) cyclopentanone, (h) cyclohexanone.

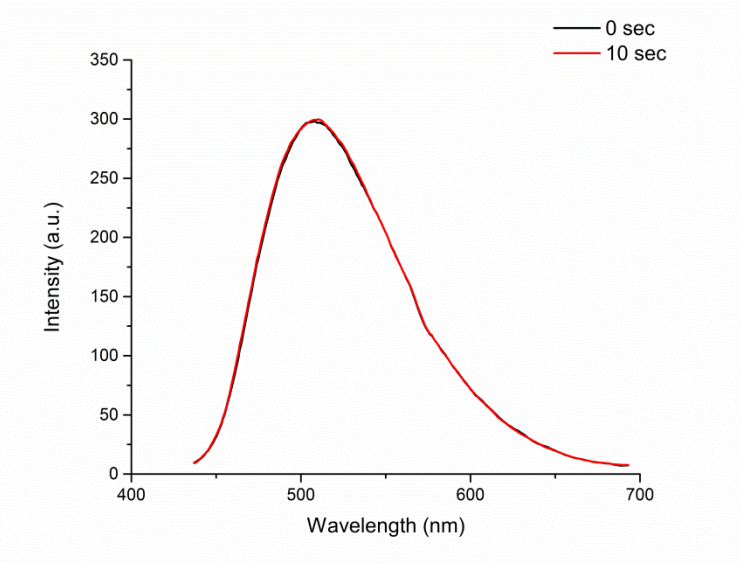

(a)

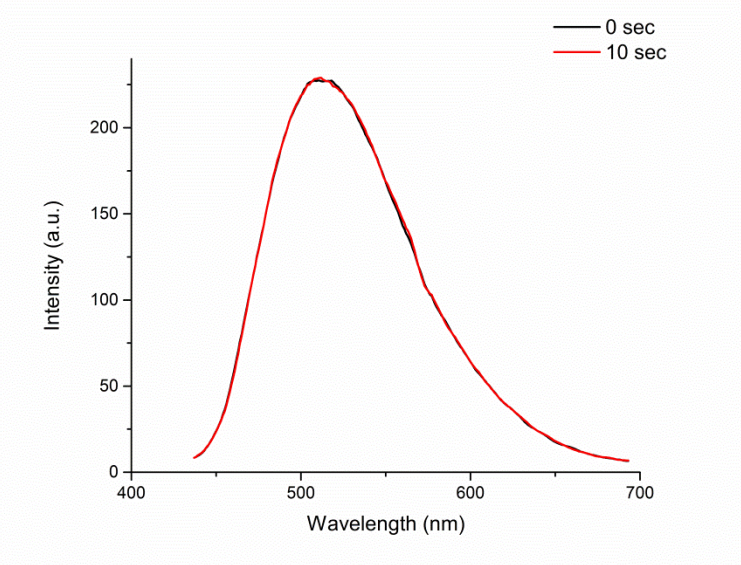
0 sec
10 sec
Intensity (a.u.)
0
50
100
150
200
400
500
600
700
Wavelength (nm)

(b)

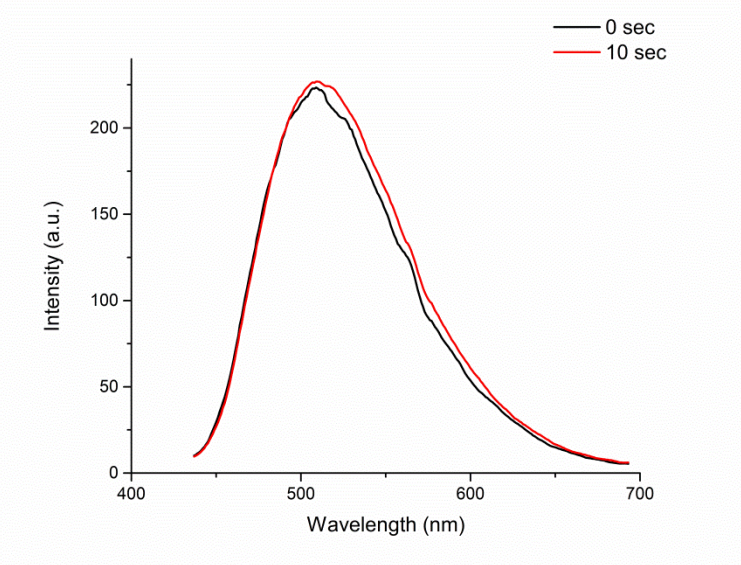
0 sec
10 sec
Intensity (a.u.)
0
50
100
150
200
400
500
600
700
Wavelength (nm)

(c)

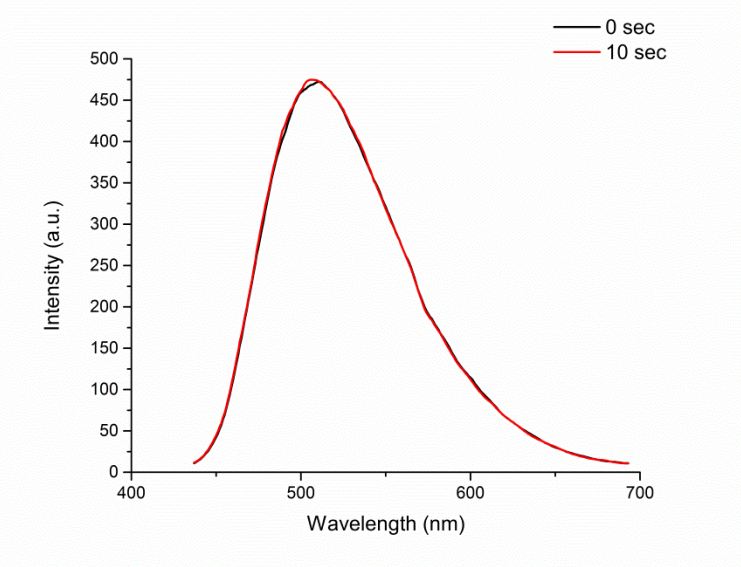
0 sec
10 sec
Intensity (a.u.)
Wavelength (nm)
0
50
100
150
200
250
300
350
400
450
500
400
500
600
700

(d)

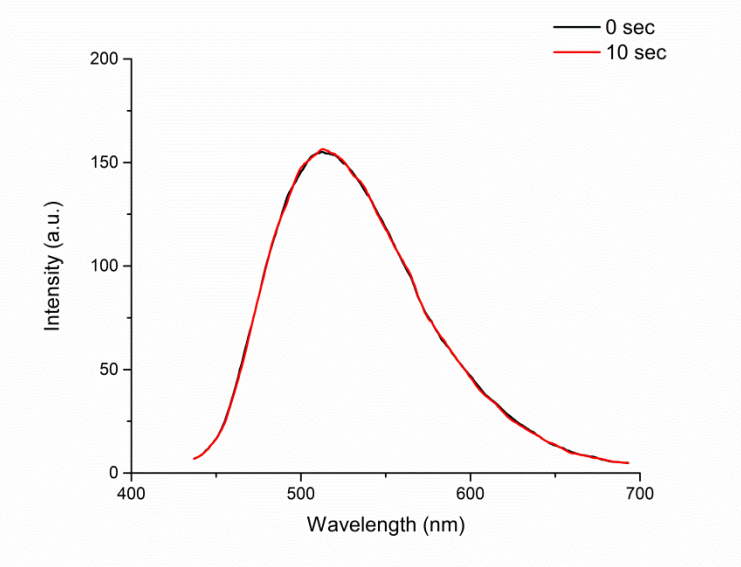
0 sec
10 sec
Intensity (a.u.)
Wavelength (nm)
0
50
100
150
200
400
500
600
700

(e)

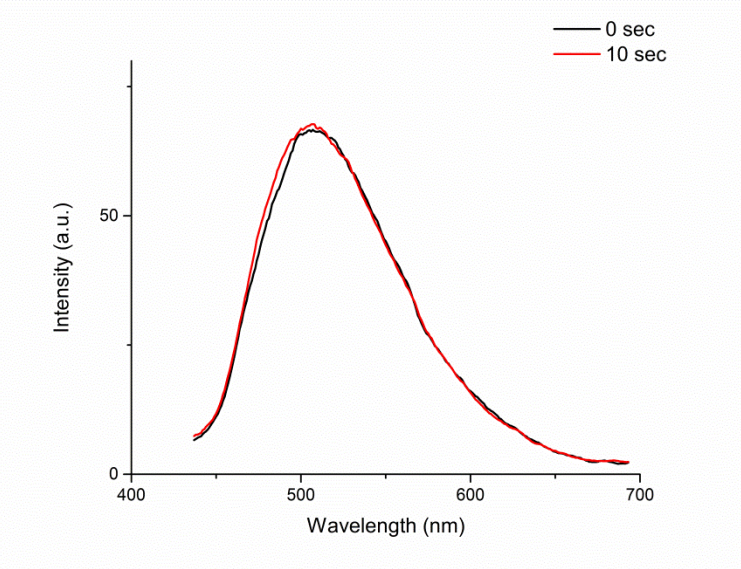
0 sec
10 sec
Intensity (a.u.)
0
50
400
500
600
700
Wavelength (nm)

(f)

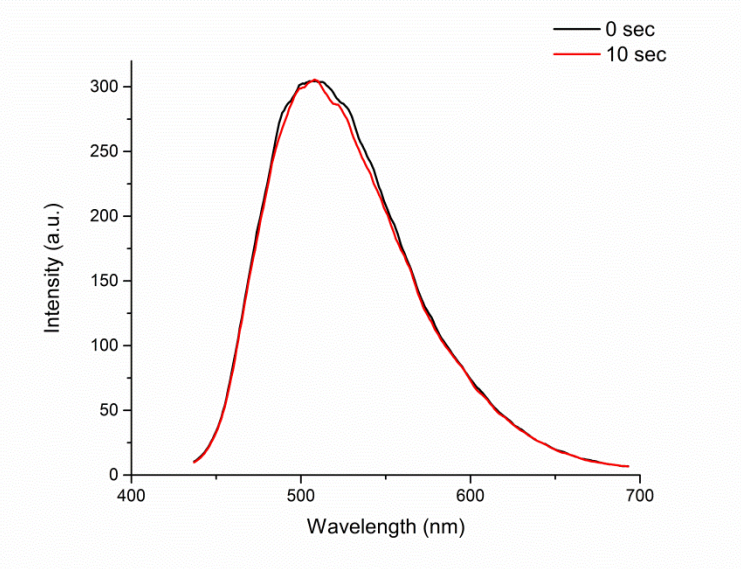
0 sec
10 sec
Intensity (a.u.)
0
50
100
150
200
250
300
400
500
600
700
Wavelength (nm)

(g)

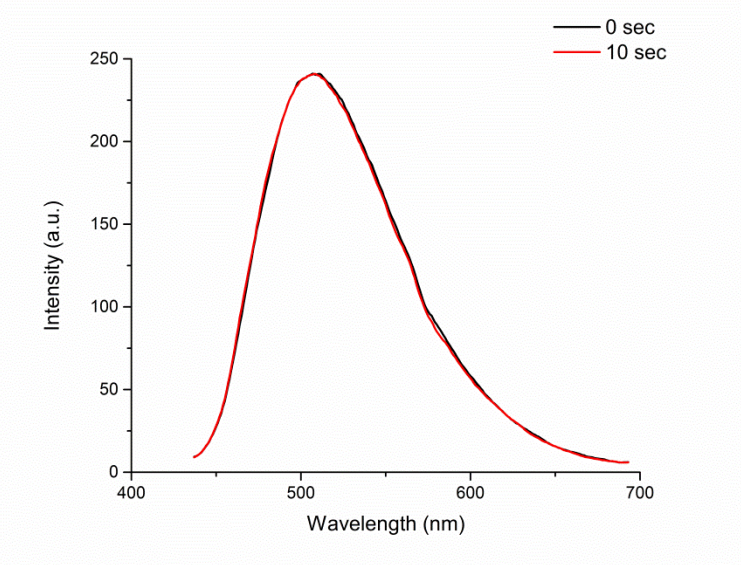

(h)

Figure S13. PL emission spectra of LMOF-201' (black) and the same sample after 10 s exposure to analytes (red) at room temperature: (a) 3-pentanone, (b) 2-octanone, (c) butanone, (d) 2,4-dimethyl-3-pentanone, (e)acetone, (f) cycloheptanone, (g) cyclopentanone, (h) cyclohexanone.

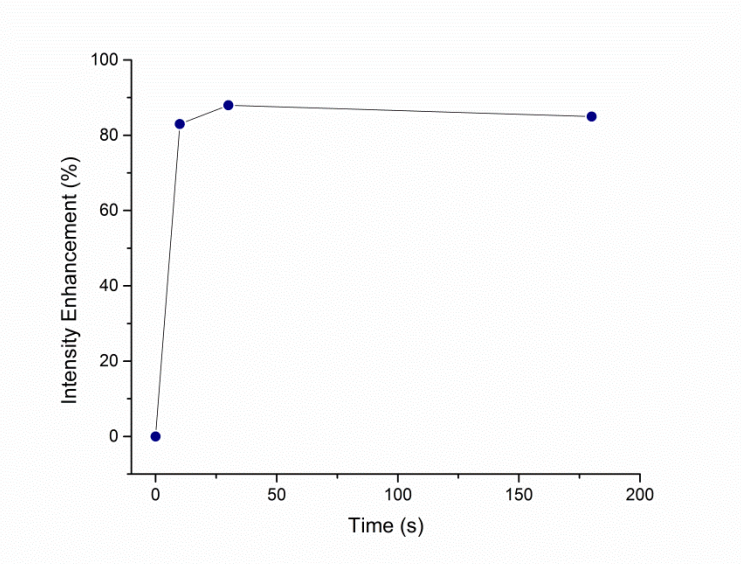

(a)

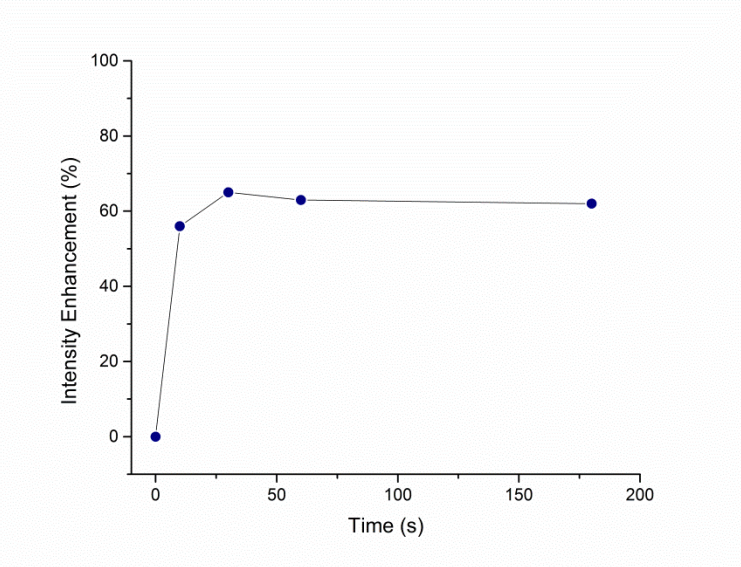

(b)

Figure S14. Time dependent emission intensity enhancement of LMOF-202' after exposure to cycloheptanone (a) and cyclohexanone (b) at room temperature.

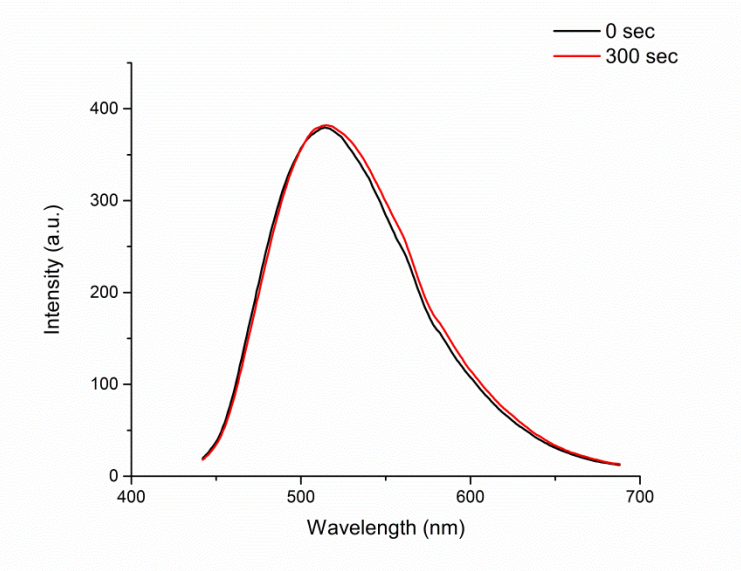

Figure S15. PL emission spectra of LMOF-201' (black) and the same sample after 300 s exposure to dry RDX (red) at room temperature.

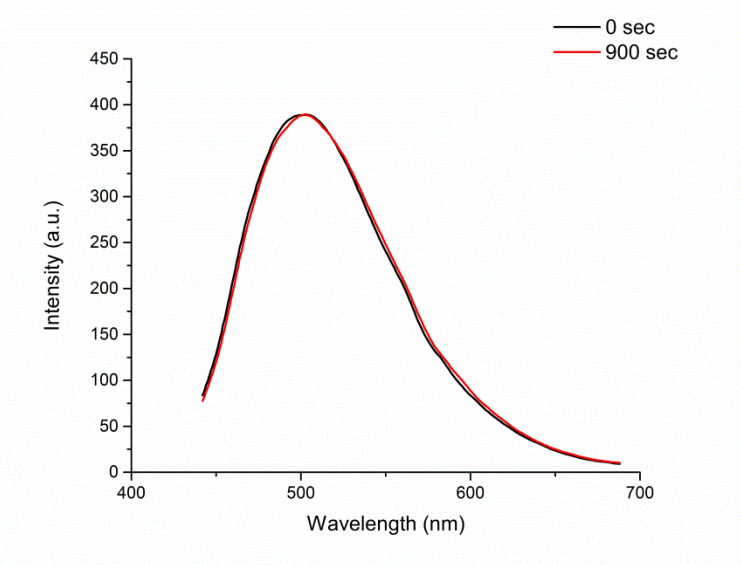

Figure S16. PL emission spectra of LMOF-202’ (black) and the same sample after 900 s exposure to dry RDX (red) at room temperature.

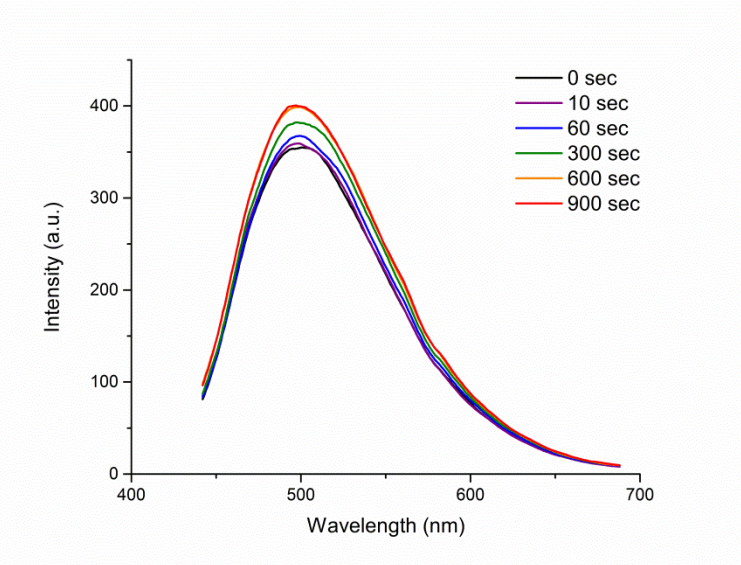

(a)

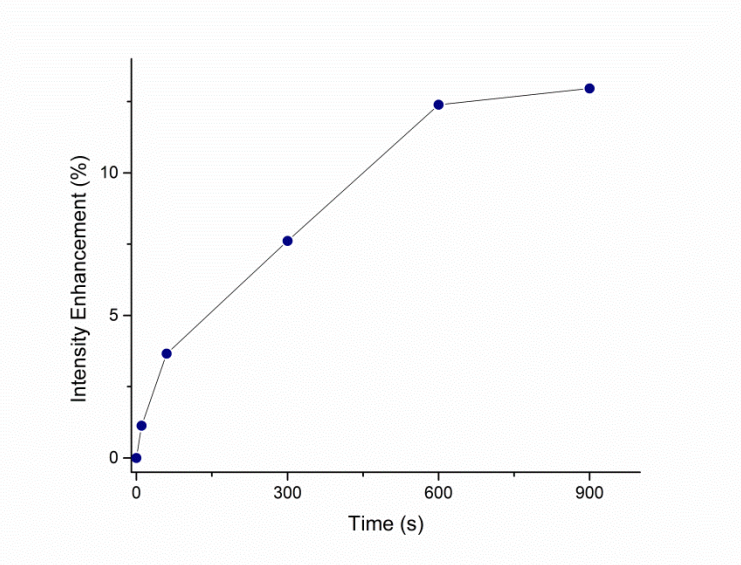

(b)

Figure S17. (a) PL emission spectra of LMOF-202' (black) and the same sample after gradual exposure to a RDX sample freshly recrystallized in cyclohexanone (red) at room temperature. (b) The time dependent emission intensity enhancement of the process showing in (a).

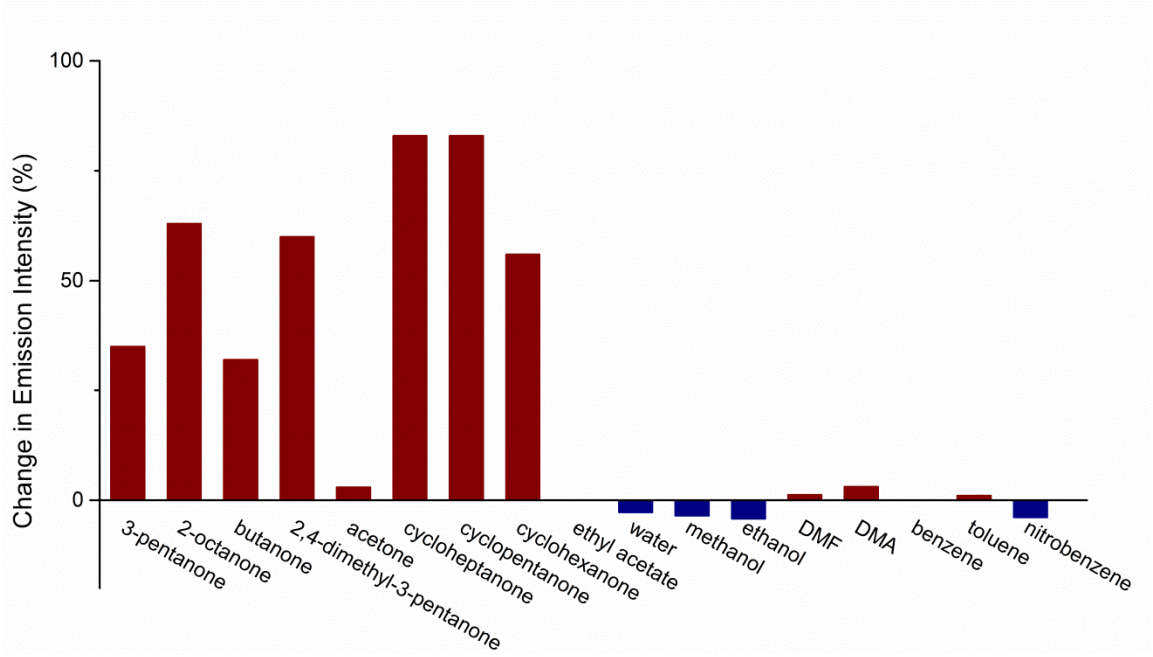

Figure S18. A summary of the emission intensity change of LMOF-202' after exposure to analytes for 10 s at room temperature.

6. Fluorescence Titration of DNT

Powder samples of LMOF-121 and -202 were dispersed in DMF under ultra-sonication to afford 4 mg/mL suspensions respectively. 10 μL of 0.001 M DNT aliquots (in DMF) were added to a quartz cuvette containing 4 mL LMOF suspension. Stirring was applied to ensure a uniform dispersion. Fluorescence spectra were recorded with the incremental addition of DNT aliquots.

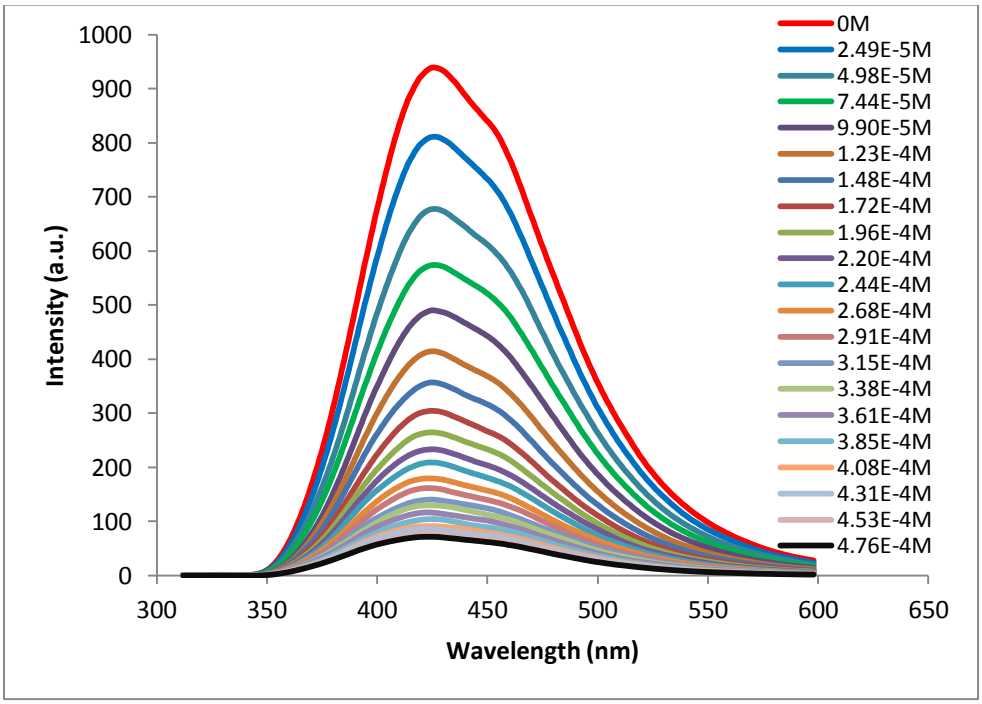

(a)

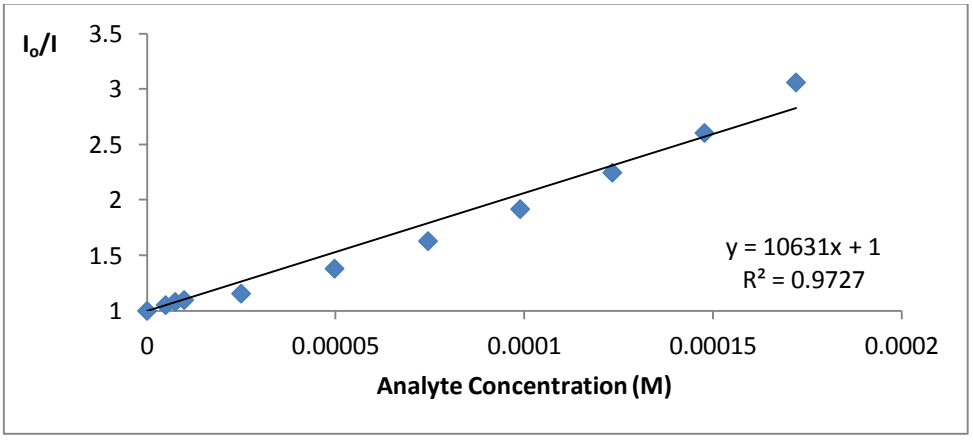

(b)

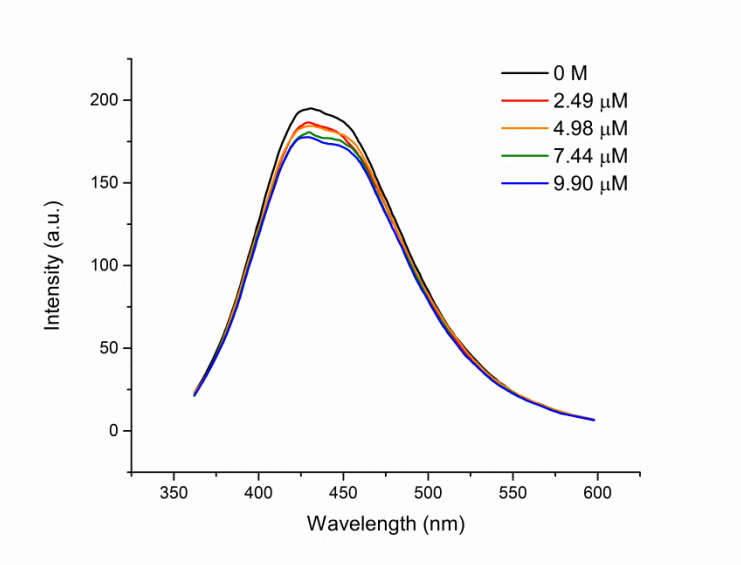

(c)

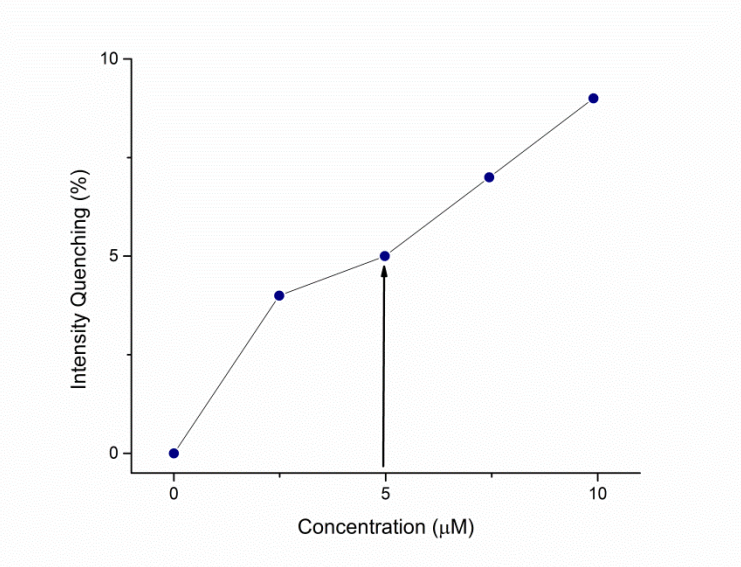

(d)

Figure S19. (a) Quenching of the fluorescence of LMOF-121 upon the incremental addition of DNT (10 μL, 0.01 M aliquot). (b) Stern-Volmer plot of LMOF-121 showing the quenching efficiency of DNT. (c) Quenching of the fluorescence of LMOF-121 upon the incremental addition of lower concentration DNT (10 μL, 0.001 M aliquot). (d) Detection limit determined from (c): DNT = 4.98 μM or 0.91 μg/mL, from this point on, a steeper slope is observed.

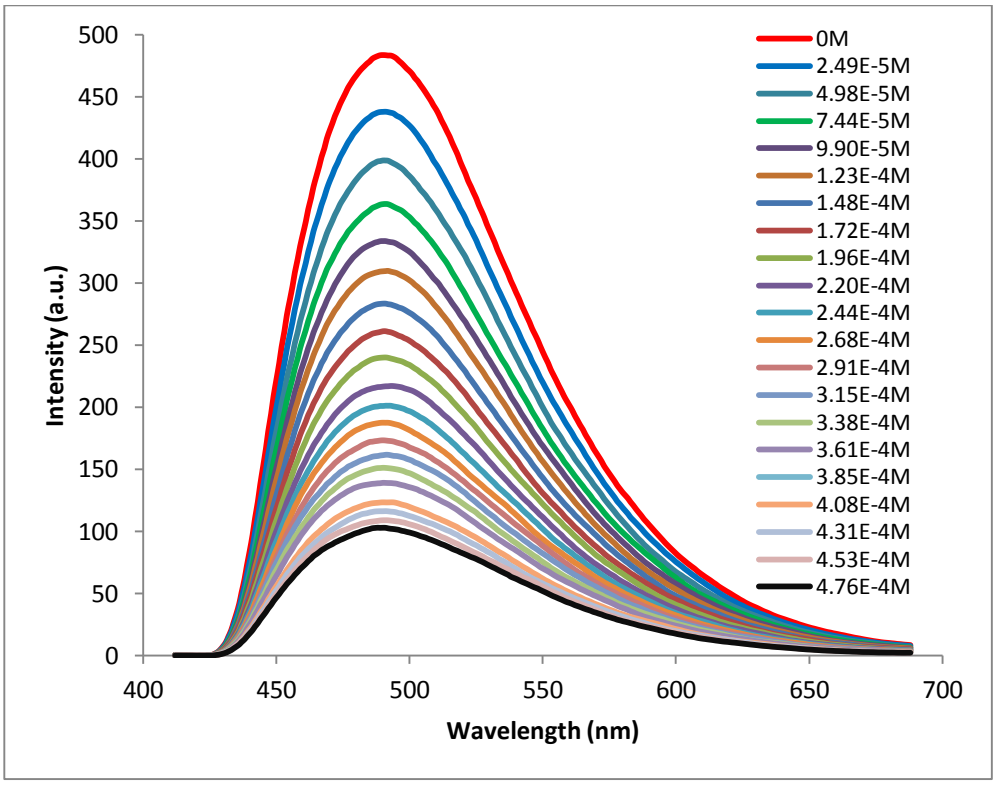

(a)

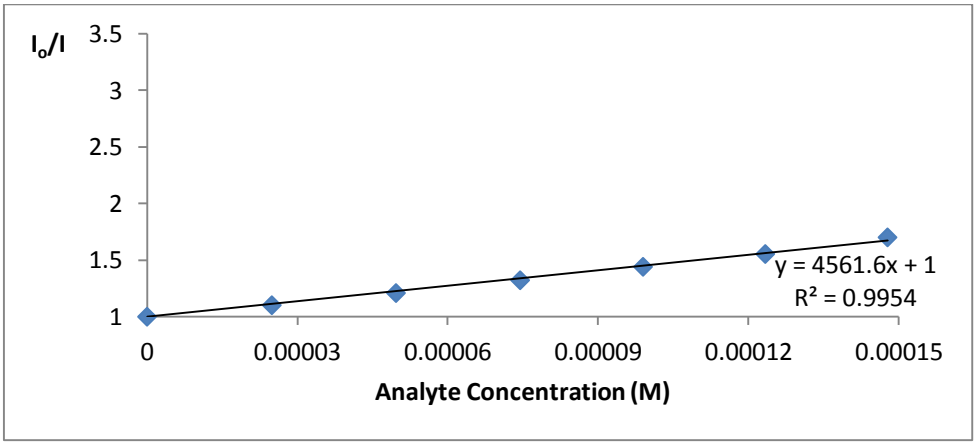

(b)

Figure S20. (a) Quenching of the fluorescence of LMOF-202 upon the incremental addition of DNT (10 μL, 0.01 M aliquot). (b) Stern-Volmer plot of LMOF-202 showing the quenching efficiency of DNT.

7. Molecular Orbital and Band Structure Calculations

The electronic properties of LMOFs and ketone analytes were studied utilizing the density functional theory (DFT) computation. Gaussian 09 suite of programs[4] and a hybrid functional, B3LYP[5-7] were employed. For LMOFs, the paddle-wheel SBU (two Zn^{2+} ions, four carboxylates, two bpy ligands) was chosen as a model. Dangling bonds were terminated by hydrogens. The full electron basis set DGDZVP[8, 9] was applied to LMOFs. For comparison purpose, LMOFs were also computed with basis sets SDD[10, 11] (Zn), 6-31G*, and 6-31+G*[12-23] (H, C, N, O). Ketones were computed with basis sets DGDZVP and 6-31+G*. Band structure and density of state calculations of LMOF-121 and LMOF-202 were also performed employing Extended Hückel method.[24, 25]

Table S6. Calculated CB and VB levels of LMOFs (SBU model) using DFT method.

Method	B3LYP								
Basis Set	DGDZVP			SDD, 6-31G*			SDD, 6-31+G*		
Compound	VB (eV)	CB (eV)	ΔE	VB (eV)	CB (eV)	ΔE	VB (eV)	CB (eV)	ΔE
LMOF-121	-6.121	-2.128	3.993	-5.829	-1.780	4.049	-6.129	-2.108	4.021
LMOF-201	-6.283	-2.645	3.639	-5.991	-2.298	3.694	-6.290	-2.612	3.677
LMOF-202	-5.772	-2.404	3.369	-5.510	-2.054	3.455	-5.780	-2.379	3.401

Table S7. Calculated CB minimum and VB maximum of LMOFs (full crystal structure) using Extended Hückel method.

Compound	VB (eV)	CB (eV)	ΔE (eV)
LMOF-121	-11.974	-9.348	2.626
LMOF-202	-12.043	-9.740	2.302

Table S8. Calculated HOMO and LUMO energy levels of ketones.

Method	B3LYP			
Basis Set	DGDZVP		6-31+G*	
Name	HOMO (eV)	LUMO (eV)	HOMO (eV)	LUMO (eV)
3-pentanone	-6.893	-0.547	-6.921	-0.630
2-octanone	-6.884	-0.559	-6.932	-0.663
butanone	-6.935	-0.587	-6.972	-0.682
2,4-dimethyl-3-pentanone	-6.707	-0.611	-6.731	-0.717
acetone	-6.985	-0.640	-7.027	-0.746
cycloheptanone	-6.681	-0.577	-6.734	-0.768
cyclopentanone	-6.753	-0.723	-6.790	-0.834

cyclohexanone	-6.692	-0.631	-6.742	-0.839

Table S9. Calculated HOMO and LUMO energy levels of selected analytes at B3LYP/6-31+G*.

Group	Chemical Nature	Name	HOMO (eV)	LOMO (eV)
A	Electron Deficient Conjugated	cyanobenzene	-7.552	-1.790
		2-nitrotoluene (NT)	-7.555	-2.747
		1,4-dicyanobenzene	-8.029	-2.871
		nitrobenzene (NB)	-7.888	-2.915
		2,4-dinitrotoluene (DNT)	-8.414	-3.409
		1,3-dinitrobenzene (*m*-DNB)	-8.731	-3.597
		2,4,6-trinitrotoluene (TNT)	-8.810	-3.930
		1,4-benzoquinone	-7.798	-3.948
		1,4-dinitrobenzene (*p*-DNB)	-8.661	-3.955
		picric acid (PA)	-8.595	-4.321
B	Electron Rich Aromatic	durene	-6.097	-0.065
		mesitylene	-6.429	-0.190
		o-xylene	-6.504	-0.205
		m-xylene	-6.491	-0.262
		aniline	-5.718	-0.282
		4-ethyltoluene	-6.399	-0.287
		p-xylene	-6.391	-0.310
		toluene (TO)	-6.675	-0.348
		ethylbenzene (Et-BZ)	-6.635	-0.360
		anisole	-6.163	-0.374
		benzene (BZ)	-6.995	-0.393
		phenol	-6.314	-0.482
		chlorobenzene (Cl-BZ)	-6.946	-0.776
		bromobenzene (Br-BZ)	-6.841	-0.787
C	Electron Deficient Aliphatic	nitroethane (NE)	-8.396	-2.331
		1-nitropropane (NP)	-8.339	-2.331
		nitromethane (NM)	-8.508	-2.486
		2,3-dimethyl-dinitrobutane (DMNB)	-8.620	-2.853
		trinitroglycerin (TNG)	-9.494	-2.934
		1,3,5-trinitroperhydro-1,3,5-triazine (RDX)	-8.926	-2.959
		octahydro-1,3,5,7-tetranitro-1,3,5,7-tetrazocine (HMX)	-8.740	-3.053
D	Others	water	-8.736	0.684
		methanol	-7.669	0.008
		ethyl acetate	-7.650	0.008
		ethanol	-7.569	0.005
		N,N-dimethylacetamide (DMA)	-6.700	-0.084
		N,N-dimethylformamide (DMF)	-6.926	-0.084
		butyronitrile	-8.967	-0.138
		acetonitrile	-9.185	-0.261
		3-pentanone	-6.921	-0.630
		2-octanone	-6.932	-0.663
		butanone	-6.972	-0.682
		2,4-dimethyl-3-pentanone	-6.731	-0.717
		acetone	-7.027	-0.746
		cycloheptanone	-6.734	-0.768
		cyclopentanone	-6.790	-0.834
		cyclohexanone	-6.742	-0.839
		chloroform	-8.742	-1.623

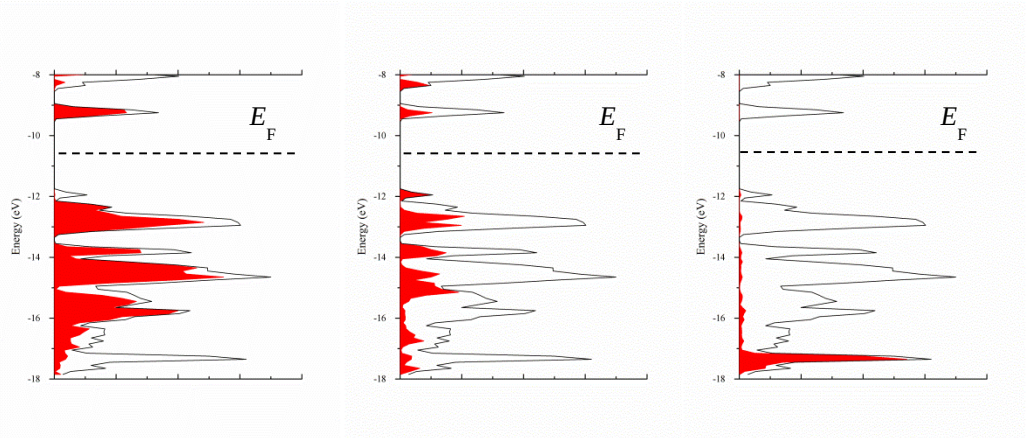

Figure S21. Calculated density of states (*DOS*) for LMOF-121 using Extended Hückel method. The solid curve denotes the total *DOS*. The shaded area refers to the contribution from oba (left), bpy (middle), and Zn (right) respectively. The dashed horizontal line denotes the Fermi level.

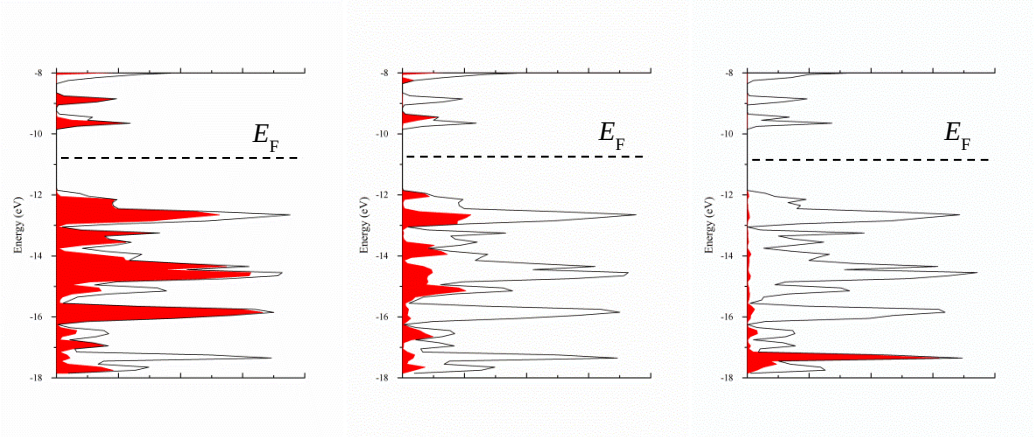

Figure S22. Calculated density of states (*DOS*) for LMOF-202 using Extended Hückel method. The solid curve denotes the total *DOS*. The shaded arearefers to the contribution from hfdc (left), bpy (middle), and Zn (right) respectively. The dashed horizontal line denotes the Fermi level.

8. In-situ IR spectroscopy to study of ketone molecules adsorption

A powder sample of MOF compound (~2 mg) was pressed onto a KBr pellet. The pellet was activated under N_2 flow at elevated temperature above 140˚C and then placed into a high pressure cell purchased from Specac at the focal point of the sample compartment of the infrared spectrometer (Nicolet 6700, Thermo Scientific) equipped with a liquid N_2–cooled MCT-A detector.[26, 27] The measurements have been performed

in transmission mode between 650 and 4000 cm^{-1} (4 cm^{-1} spectral resolution). One ZnSe window was open for vapor exposure experiments. The reference spectra were recorded on the activated MOF sample under N_2 purge at room temperature (See Figure S23 for the pure MOF spectra). The ketone molecule vapors were then slightly brought into the MOF sample by N_2 carrier gas for 3 min through the open window. Spectra were again collected after ketone vapor exposure under N_2 purge. The cell was also connected to a vacuum line for evacuation. For the vapor phase spectra, a pure KBr pellet was used and vapors of analytes (acetone, 2-octanone, cyclopentanone, cyclohexanone) were introduced into the evacuated cell for collecting the spectra of the vapor phase (See Figure S24). The assignments were done based on the refs [28-32].

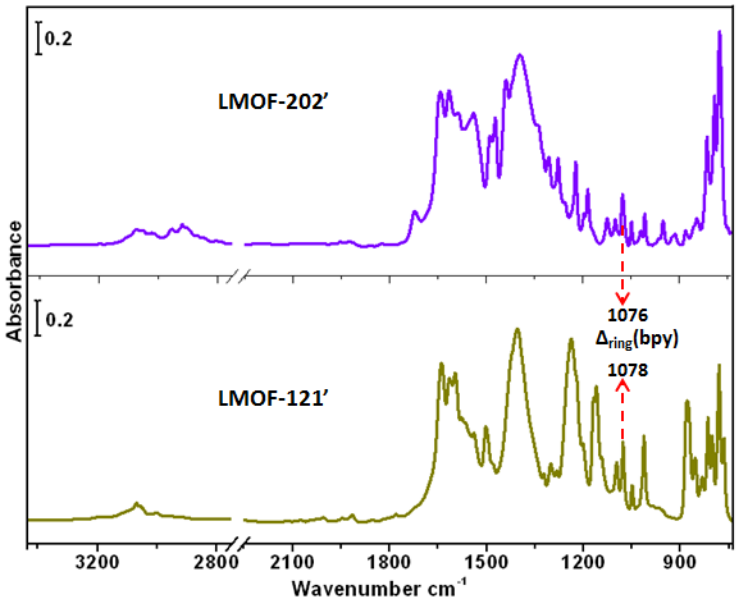

Figure S23. IR absorption spectra of activated (top) LMOF-202' and (bottom) LMOF-121' reference to KBr pellet under N_2 purge.

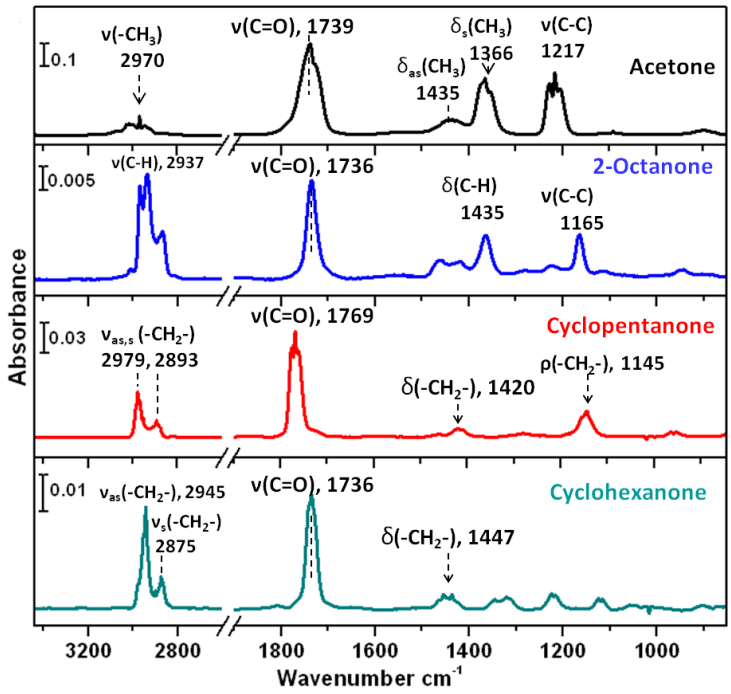

Figure S24. IR absorption spectra of vapor phase analytes from top to bottom: acetone, 2-octanone, cyclpentanone, cyclohexanone.

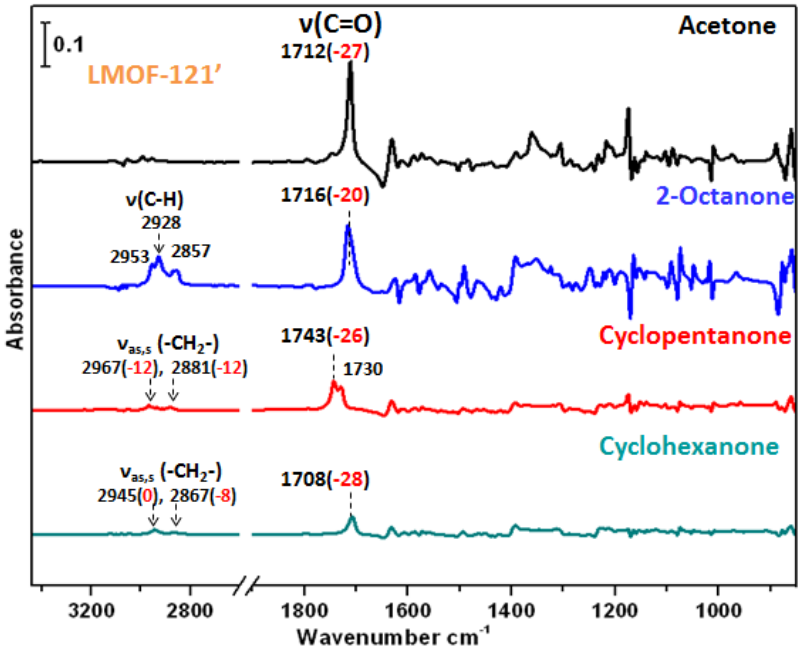

Figure S25. IR absorption spectra of adsorbed ketone molecules: acetone, 2-octanone, cyclopentanone, cylcohexanone in LMOF-121' referenced to the IP spectrum of blank LMOF-121'.The spectra were recorded after exposing LMOF samples to vapors for 3 min.

Table S10. Relative intensities of ν(C=O) bands for the ketone molecules adsorbed in LMOF-202' and LMOF-121'.

ν(C=O)	$I_{\nu(C=O)}/ I_{\delta ring}$	
	LMOF-202'	LMOF-121'
Acetone	1.098	1.000
2-Octanone	1.238	0.7013
Cyclopentanone	1.330	0.4137
Cyclohexanone	1.043	0.2133

All bands are normalized to in-plane 4,4'-bipy ring deformation mode δ_{ring} at 1076 for LMOF-202' and 1078 cm^{-1} for LMOF-121'.

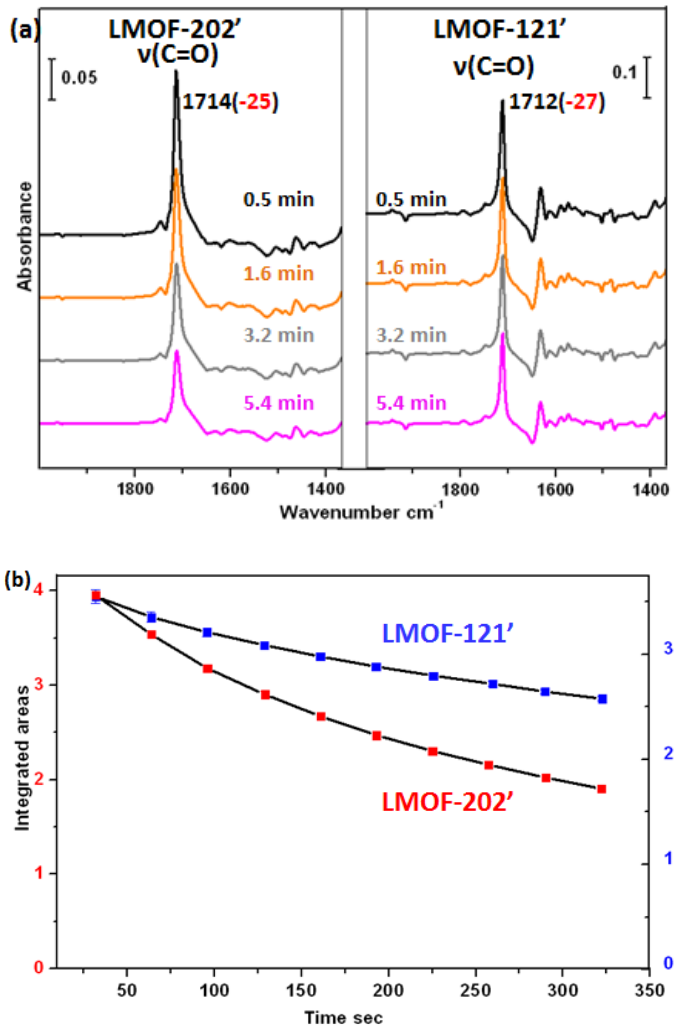

Figure S26. (a) IR spectra of adsorbed acetone in LMOF-202' (left) and LMOF-121' (right) under N_2 purge as a function of time. (b) Integrated areas of ν(C=O) band of adsorbed acetone decrease as a function of time. Blue, LMOF-121'; red, LMOF-202'.

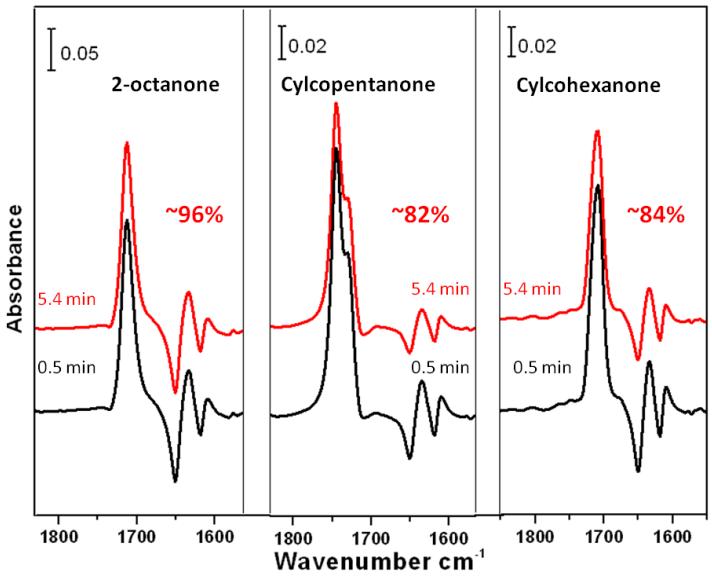

Figure S27. Time-dependent IR spectra of adsorbed 2-octanone, cyclopentanone and cyclohexanone in LMOF-202' under N_2 purge. Blue, data recorded within 0.5 min; red, after 5.4 min.

Figure 5 and Figure S25 show the IR absorption spectra upon adsorption of acetone, 2-octanne, cyclopentanone, cyclohexanone into two LMOF-202' and LMOF-121'. The spectra show clearly that ketone molecules are adsorbed into the MOFs. The main features of adsorbed ketone molecules are the bands around 1700 to 1750 cm^{-1}, which can be attributed to the stretching modes of carbonyl groups and the bands around 2800 to 3000 cm^{-1}, assigned to the C-H stretching modes.[28, 29] Compared to the vapor phase spectra shown in Figure 21, the ν(C=O) bands are red shifted (~20 to 30 cm^{-1}) after adsorption into the MOFs compounds for all the ketone molecules. This modest red shift indicates that these molecules are physically adsorbed into MOFs.[28, 29, 32] After purging under N_2 flow at room temperature, the amount of adsorbed species gradually decreases as shown in Figure S26 and S27. The incorporation of ketone molecules 2-octanone, cyclopentanoe, cyclohexanone (with the exception of acetone) causes significant perturbations to the skeleton vibrational modes of LMOF-202',[27] especially in the range of 1200 to 1700 cm^{-1} that includes carboxylate group stretching modes $\nu_{as,s}(COO^-)$, phenyl and pyridine ring stretching modes ν(C=C), ν(C=N), and C-H bending modes β(C-H) as shown in Figure 5. The lower perturbation induced by acetone adsorption suggests that the interaction between acetone and MOF is weaker than that induced by the other three molecules. On the contrary, acetone causes significant perturbations to the skeleton vibrational modes of LMOF-121' as shown in Figure 25.

To quantify and compare the adsorption of ketone molecules trapped inside the two MOFs, we normalized the intensities of ν(C=O) modes to in-plane 4,4'-bpy ring deformation mode δ_{ring} existing in both LMOF-202' and LMOF-121' (see Table S10).[33] It is clear that the amount of adsorption for 2-octanone, cyclopentanoe, cyclohexanone in LMOF-202' is much higher than that in LMOF-121', especially for cyclopentanone and cyclohexanone. This could be another reason for the rather low fluorescence enhancement observed upon adsorption of these two molecules in LMOF-121'. For the adsorbed acetone, the adsorption is similar in both MOF structures at the very beginning (0.5 min). However, the adsorbed molecules are gradually removed from the frameworks under N_2 purge as shown in Figure S26. In LMOF-202', the desorption is faster than in LMOF-121'. After 5.4 min, only around 50% remains compared to the initial recorded amount (within 0.5 min). This further shows that acetone molecules interact only weakly with the LMOF-202' frameworks and can therefore diffuse easily out of the structure. The capability of LMOF-202' to retain the other three molecules 2-octanone, cyclopentanone and cyclohexanone is higher. After 5.4 min, 96%, 82%, and 84% are left compared to the initial recorded amount (within 0.5 min) as shown in Figure S27.

In summary, the infrared absorption data indicates that all these molecules are adsorbed into the MOFs structures, that the amount of adsorption into LMOF-202' is higher than in LMOF-121', and that the molecules are perturbed enough (as evidence by frequency shifts) that electron transfer phenomena could take place in the excited state.

9. References

1. S. Pramanik, C. Zheng, X. Zhang, T. J. Emge and J. Li, *J. Am. Chem. Soc.*, 2011, **133**, 4153-4155.
2. G. M. Sheldrick, SHELX-97, Program for Structure Refinement, University of Göettingen, Germany, 1997.
3. A. L. Spek, PLATON, A multipurpose crystallographic tool ; Utrecht University: Utrecht, The Netherlands, 2001.
4. M. J. Frisch, G. W. Trucks, H. B. Schlegel, G. E. Scuseria, M. A. Robb, J. R. Cheeseman, G. Scalmani, V. Barone, B. Mennucci, G. A. Petersson, H. Nakatsuji, M. Caricato, X. Li, H. P. Hratchian, A. F. Izmaylov, J. Bloino, G. Zheng, J. L. Sonnenberg, M. Hada, M. Ehara, K. Toyota, R. Fukuda, J. Hasegawa, M. Ishida, T. Nakajima, Y. Honda, O. Kitao, H. Nakai, T. Vreven, J. J. A. Montgomery, J. E. Peralta, F. Ogliaro, M. Bearpark, J. J. Heyd, E. Brothers, K. N. Kudin, V. N. Staroverov, T. Keith, R. Kobayashi, J. Normand, K. Raghavachari, A. Rendell, J. C. Burant, S. S. Iyengar, J. Tomasi, M. Cossi, N. Rega, J. M. Millam, M. Klene, J. E. Knox, J. B. Cross, V. Bakken, C. Adamo, J. Jaramillo, R. Gomperts, R. E. Stratmann, O. Yazyev, A. J. Austin, R. Cammi, C. Pomelli, J. W. Ochterski, R. L. Martin, K. Morokuma, V. G. Zakrzewski, G. A. Voth, P. Salvador, J. J. Dannenberg, S. Dapprich, A. D. Daniels, O. Farkas, J. B. Foresman, J. V. Ortiz, J. Cioslowski and D. J. Fox, Gaussian 09, Revision C.01, Gaussian, Inc., Wallingford CT, 2010.
5. A. D. Becke, *Physical Review A*, 1988, **38**, 3098-3100.

6. C. Lee, W. Yang and R. G. Parr, *Physical Review B*, 1988, **37**, 785-789.
7. A. D. Becke, *J. Chem. Phys.*, 1993, **98**, 5648-5652.
8. N. Godbout, D. R. Salahub, J. Andzelm and E. Wimmer, *Can. J. Chem.*, 1992, **70**, 560-571.
9. C. Sosa, J. Andzelm, B. C. Elkin, E. Wimmer, K. D. Dobbs and D. A. Dixon, *J. Phys. Chem.*, 1992, **96**, 6630-6636.
10. T. H. D. Jr. and P. J. Hay, *Modern Theoretical Chemistry*, Plenum, New York, 1976.
11. M. Dolg, U. Wedig, H. Stoll and H. Preuss, *The Journal of Chemical Physics*, 1987, **86**, 866-872.
12. R. Ditchfield, W. J. Hehre and J. A. Pople, *The Journal of Chemical Physics*, 1971, **54**, 724-728.
13. W. J. Hehre, R. Ditchfield and J. A. Pople, *The Journal of Chemical Physics*, 1972, **56**, 2257-2261.
14. P. C. Hariharan and J. A. Pople, *Theoret. Chim. Acta*, 1973, **28**, 213-222.
15. P. C. Hariharan and J. A. Pople, *Mol. Phys.*, 1974, **27**, 209-214.
16. M. S. Gordon, *Chem. Phys. Lett.*, 1980, **76**, 163-168.
17. M. M. Francl, W. J. Pietro, W. J. Hehre, J. S. Binkley, M. S. Gordon, D. J. DeFrees and J. A. Pople, *The Journal of Chemical Physics*, 1982, **77**, 3654-3665.
18. R. C. Binning and L. A. Curtiss, *J. Comput. Chem.*, 1990, **11**, 1206-1216.
19. J.-P. Blaudeau, M. P. McGrath, L. A. Curtiss and L. Radom, *The Journal of Chemical Physics*, 1997, **107**, 5016-5021.
20. V. A. Rassolov, J. A. Pople, M. A. Ratner and T. L. Windus, *The Journal of Chemical Physics*, 1998, **109**, 1223-1229.
21. V. A. Rassolov, M. A. Ratner, J. A. Pople, P. C. Redfern and L. A. Curtiss, *J. Comput. Chem.*, 2001, **22**, 976-984.
22. T. Clark, J. Chandrasekhar, G. W. Spitznagel and P. V. R. Schleyer, *J. Comput. Chem.*, 1983, **4**, 294-301.
23. M. J. Frisch, J. A. Pople and J. S. Binkley, *The Journal of Chemical Physics*, 1984, **80**, 3265-3269.
24. R. Hoffmann, *J. Chem. Phys.*, 1963, **39**, 1397-1412.
25. M.-H. Whangbo, R. Hoffmann and R. B. Woodward, *Proceedings of the Royal Society of London. A. Mathematical and Physical Sciences*, 1979, **366**, 23-46.
26. N. Nijem, J.-F. Veyan, L. Kong, K. Li, S. Pramanik, Y. Zhao, J. Li, D. Langreth and Y. J. Chabal, *J. Am. Chem. Soc.*, 2010, **132**, 1654-1664.
27. K. Tan, N. Nijem, P. Canepa, Q. Gong, J. Li, T. Thonhauser and Y. J. Chabal, *Chem. Mater.*, 2012, **24**, 3153-3167.
28. A. Panov and J. J. Fripiat, *Langmuir*, 1998, **14**, 3788-3796.
29. M. El-Maazawi, A. N. Finken, A. B. Nair and V. H. Grassian, *J. Catal.*, 2000, **191**, 138-146.
30. N. Fuson, M.-L. Josien and E. M. Shelton, *J. Am. Chem. Soc.*, 1954, **76**, 2526-2533.
31. R. Cataliotti and G. Paliani, *Chem. Phys. Lett.*, 1973, **20**, 280-283.
32. S. Scirè, C. Crisafulli, R. Maggiore, S. Minicò and S. Galvagno, *Appl. Surf. Sci.*, 1996, **93**, 309-316.
33. A. Topaçli and S. Akyüz, *Spectrochimica Acta Part A: Molecular and Biomolecular Spectroscopy*, 1995, **51**, 633-641.